Compatibility of different forms of recycled composite filaments for use in 3D printing

By

Mazin Tahir

Master of Engineering - Thesis

Structures and Composite Materials Laboratory

Department of Mechanical Engineering

McGill University, Montreal

A Thesis Submitted to the Faculty of Graduate Studies and Research in Partial Fulfilment of the Requirements for the Degree of Master of Engineering

Dedicated to ...

My Parents

``While you are in the life journey, don`t forget who you are and what is your destination``.

`Zain

Abstract

Aerospace, automotive, renewable energy and a wide range of other sectors are using Composite materials. With almost no emissions during operation, the wind energy sector is considered a promising solution for a future energy demand that is accompanied by more strict regulations on sustainability and environmental concerns. However, waste from hundreds of thousands of non-recyclable end-of-life wind turbine blades will be generated within the next decades. The manufacturing methods used to fabricate composite materials makes it challenging to recycle them. The non-recyclable nature of thermoset matrix composite materials is a major parameter in this complex issue. Unfortunately, most of the proposed recycling methods, thus far, have failed to establish a well-defined cost-effective process that is both sustainable and scalable to the industrial level. This work studied the effect of epoxy debris on the strength and stiffness of PLA reinforced Ground Recycled Fibres (GRF) composites that are used in Fused Deposition Modeling (FDM) 3D printing. Three different fibre categories (i.e. virgin, ground and pyrolyzed fibres) were examined and compared. An end-of-life wind blade was first cut into small pieces that were then fed into a hammer-mill grinder to convert them into short fibres and powder. Then, a multi-level sieving machine was used to sort and grade the powder into different size ranges. Single fibre tensile tests at different gauge lengths and pull-out interfacial strength tests were performed at the fibre-level to fully establish the Halpin-Tsai short fibre theoretical model. Then, an ASTM D638 tensile test was performed on different PLA coupons prepared with the three fibre categories and with different fibre contents between 3, 5% and 10% to validate the suggested theoretical models. Compared to virgin fibres, both recycled fibres, i.e. ground and pyrolyzed fibres, exhibit higher strength and stiffness values. As a result, using recycled fibreglass to reinforce PLA could be not only an environmentally promising solution, but also a competitive candidate to other 3D printing materials in the market. More precisely, ground recycled fibres (GRF) showed higher ultimate tensile strength compared to pyrolyzed ones. While contrarily higher stiffness values were obtained for Pyrolyzed fibres compared to ground fibres. A significant deviation from the theoretical model was observed on ground fibre/PLA coupons response compared to pyrolyzed fibres. A full comparison, in terms of strength and stiffness of the different tested fibre categories, will highlight and present the most potential feasible solution to reinforce PLA filaments.

Keywords: Short fibre, Rule of Mixtures, Halpin-Tsai, Cox, Recycling, wind turbine blades, FDM.

RÉSUMÉ

Les matériaux composites sont utilisés pour de nombreuses applications autant dans l'industrie automobile qu'àérospatiale que des énergies renouvelables. Avec presque aucune émission pendant le fonctionnement, l'énergie éolienne est considérée comme une solution prometteuse en vue de la future demande énergétique qui sera accompagnée par des régulations de durabilité et environnementales plus strictes. Cependant, plusieurs études ont montré que les déchets provenant de pâles d'éoliennes non recyclables vont augement exponentiellement dans les prochaines décennies. La nature éclectique de matériaux composites représente un défi face à leur recyclage. Les matériaux à matrice thermodurcissable ne sont pas recyclables, ce qui amène un défi supplémentaire à ce problème complexe.

Les méthodes de recyclage de composites trouvées dans la littérature peuvent être catégoriser en plusieurs approches: mécanique, thermique ou chimique. Malheureusement, la plupart des méthodes proposées jusqu'à maintenant ont échoué à établir un procédé abordable en terme de coûts qui puisse être adapté au niveau industriel. Ce projet étudie l'effet de débris d'époxy sur la solidité et la rigidité de composites en PLA renforcés par des fibres recyclées qui seront utilisés en impression 3D.

Acknowledgement

First and foremost, to the most precious persons in my entire life, my father and my mother, for working so hard on breading me on to reach this level delivering the final piece representing my academia life so far. The unforgettable nights, tiredness and indeed the energy dedicated will ever be appreciated.

I can not fully express my gratitude to my supervisor, Larry Lessard, for his generosity, guidance, and indeed the faith he believed to deliver part of his lab project to be accomplished by me. My thanks to the initial core that always supported me, with high level of assistance, my lab team, it was such a pleasure working and cooperating with every single member of you, and for sure the merit of exchanging and passing on ideas with such a talented people was incomparable.

Along with the academic individuals, I should never forget the most reason of pursuing my M.Eng degree, AGFE foundation, with all aspects of help delivered by them, not only financial, but also the persistent mentoring, advising and the network of bright scholars existed with in its body structure, thank you so much.

And finally, I would be remiss if I did not mention the sweetest hearted friends I met here in Montreal, from diverse backgrounds and communities, they added a flavor for these two years making them more than documented deep in my heart.

Table of Contents

List of Figures

List of Tables

1. Introduction

Composite materials are a type of material composed of two main elements, matrix and reinforcement. As a result of their high strength- and stiffness-to-weight ratios, they are used to design structures with considerably lower energy use and lower carbon footprint [1,2]. Recently, continuing improvements in the manufacturing processes and materials processing of composites have led to an increasingly growing use of composites in a wide variety of applications, such as aerospace, military and sporting products. Wind energy is another major application of composites with an extensive use of glass fibre reinforced plastics (GFRP) that have been used for blade manufacturing [3,4]. Recently, an extensive literature review discussed several methods for recycling GFRP. Unfortunately, the proposed recycling methods failed to establish a well-defined practice to recycle wind blades with high commercialization capacity. Furthermore, the wind energy sector is fairly young in such a way that there is a limited experience on blade recycling. Landfill and incineration are the most common routes commonly used to dispose of wind turbine blades at their end of their lifespan. While landfill is not environmentally friendly, incineration is the mainstream route proposed in the wind turbine blade disposal literature. Incineration has an advantage over landfill, because of the scrap that is toxic due to the synthetic compounds used in composites manufacturing. This toxic scrap cannot be left behind in a landfill [5-6] because landfilling blades would lead to a major production of dangerous and harmful residue materials. Furthermore, the inorganic ingredients result in the release of harmful flue gases, where tiny glass fibres create problems for dust filter devices. Recently, the recycling of wind turbine blades has been considerably investigated in the literature to resolve landfill and incineration issues [6-8]. One study showed

that the potential applications of recyclate are limited due to the lower mechanical properties of the recycled fibres, as well as their size [9]. More recently, chemical and pyrolysis methods were used to extract glass fibres from the blades of end-of-life turbines [8]. Despite the lower mechanical properties of recyclate fibres, the use of dangerous chemicals and unnecessary expense, chemical methods still show a promising outcome in terms of commercialisation [7-10]. A systematic analysis of the literature found a large amount of composites waste would be available within the next three decades [11-13]. While several studies have examined turbine blade recycling, no sustainable design practices have been suggested or implemented in the literature that reuse the materials in applications that have high potential for commercialisation. Thus, there is a need to solve the wind turbine blades waste issue [7].

As a parallel topic, Fuse Deposition Manufacturing (FDM) is the most widely used process for manufacturing pure plastic parts at a low price, with limited waste. In general, FDM 3D printing is used to develop rapid experimental prototypes, despite the relatively poor mechanical characteristics and load bearing capacities [14]. Therefore, further development of thermoplastic parts produced by FDM is important, in order to increase their usability and capabilities. One way to address this issue is to apply reinforcement materials like glass fibres to the plastic materials, thus forming glass fibre reinforced 3D printing filament [15-16]. The current project aims to define an organised approach to incorporate used end-of-life wind turbine blade materials for use in rapid prototyping (FDM). It is intended that the incorporation of recovered glass fibres in the filaments will boost the reliability and strength of the components produced by FDM and it will result in widening the applications window where those FDM materials can be applied. As mentioned earlier, the projection of re-using a huge

amount of wind turbine blade waste would lead to a major reduction in the landfilling of dangerous and harmful blade materials. Furthermore, this study will compare the mechanical performance of polylactic acid/recycled glass fibre (PLA/rGF) reinforced aligned discontinuous composites assessed experimentally and by various simple elastic micromechanical prediction models. Several discontinuous fibre models have been developed to predict the tensile properties of PLA/rGF, e.g., Rule of Mixtures, Halpin-Tsai and Cox models [75-80].

1.1. Motivation

The huge amount (details in section 2 of the thesis) of wind blade waste that will be available in the near future, accompanied with more strict regulations on landfilling and living up to the standards of circular engineering, climate change and sustainability objectives is pushing for an urgent solution for this problem. Concurrently, the rapid manufacturing 3D printing sector is gaining increased attention. 3D printing has a wide range of applications and it has been utilized in several sectors. Cheap prototyping to much more advanced industries, like medical and hybrid materials, are using 3D printing principles. Research into composite reinforced materials for 3D printing has helped to advance the processing of new and better materials. However, this rapidly advancing market has failed to provide high mechanical performance materials that could be used in advanced industries at reasonable prices.

1.2. Objectives

The primary aim of this study is to address the potential of converting recycled fiberglass waste into a more useful product by mixing the recycled fibers with PLA bioplastic in order to produce a more advanced 3D FDM printing filament. Another goal is to define all the different parameters that play a major rule in the compatibility issue and the final mechanical response

of the product. In order to accomplish the objectives, a comprehensive comparison between different pre-conditioned fibre types as well as different fibre lengths were performed to obtain the optimal conditions and the most economical feasible solution. This study will develop a framework for reusing scrap fiberglass, and transforming it into filaments that can be used in the FDM process. In addition, it is intended that the incorporation of the recovered glass fibres in the filaments will boost the reliability and strength of components produced by FDM.

1.3. Thesis organization

The thesis has been divided into five different chapters. The first chapter is the introduction where the motivation and objectives of the thesis are discussed. The second chapter provides a review of the work that has been carried out in the past. Third chapter has the detailed motivation and the approach that was used. In the fourth, fifth and sixth chapters, preliminary tests, experimental work and observations and discussion of the results were detailed, respectively. Finally, a conclusion and what can be achieved as future work is provided. Appendices are included to detail auxiliary information and present more results.

2. Literature Review

Composite materials are a type of material composed of two or more primary elements: matrix and reinforcement. Due to their high strength-to-weight and stiffness-to-weight ratios, they are used to design structures with considerably lower energy use and less carbon footprint [17-20]. Recently, further improvements in the manufacturing processes and materials knowledge of composites has led to an increasingly growing use of composites in various applications, such as aerospace, military and sporting products.

The global market for carbon fiber reinforced composites has surged approximately five times over the last decade. by 2024, the glass fiber market will have a $10 billion projected growth [22]. Industries like wind energy, printed circuit boards, pipes, tanks, and automotive components are the main contributors to this growth. Specifically, the wind energy sector is a major market of composites due to the extensive use of glass fibers in the manufacturing of wind turbine blades [23-24].

2.1. Wind energy

Wind energy is one of the main emerging sources of energy in the last two decades. Since there are no emissions released during the operation, it is considered one of the cleanest sources of energy nowadays. The total installed capacity has increased from 7600MW to 364,270MW between 1980 and the end of 2014 [25]. 14.9% of the worldwide electricity supply was projected to be secured by wind energy in 2020, according to the European Wind Energy Association [26]. Another less optimistic study done by (IEA) estimated that 15-18% of world's electricity would be supplied from wind by 2050 [27]. In the US, wind energy is expected to be one of the fastest-growing energy sources in the next years [27].

Moreover, the significant decrease in the cost of wind energy electricity makes it more competitive compared to electricity generated from fossil fuels. The average KWh price for electricity supplied by offshore wind farms had dropped by 35% in 2018 compared to 2010, according to International Renewable Energy Agency (IREA). Although there is a huge variation of the growth scenarios, this sector will keep growing rapidly to bridge the gaps between energy sources and sustainability issues [28].

Following the Paris Climate Summit in 2015, 70% of carbon emissions reduction from energy activities would be required by 2050 compared to today's levels [29]. The growth of renewable energy sources should accelerate to meet sustainability goals and maintain the average global temperatures to no more than 1.5°C [29]. Deployment of low-carbon technologies will be the critical factor for achieving effective transformation that will replace conventional fossil fuel practices and limit their use.

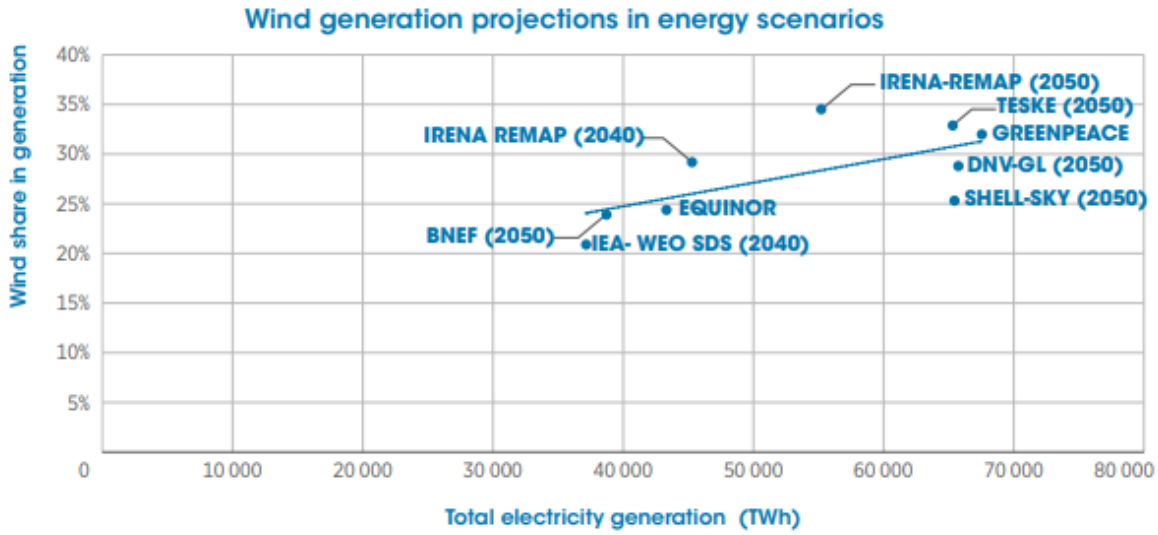

Figure 1: Wind energy growth scenarios [28]

2.2. Wind energy waste

Although wind energy is believed to produce sustainable energy without any negative environmental impacts during the operation stage, there is a down side that the energy level used in manufacturing is massive and accompanied with extensive use of chemicals [30]. Pickering and Job showed concern related to the growth of waste as a result of end-of-life disposal and how legalization is becoming more strict, thus prohibiting landfilling of Wind Turbine Blades (WTB) in some European countries [31-33].

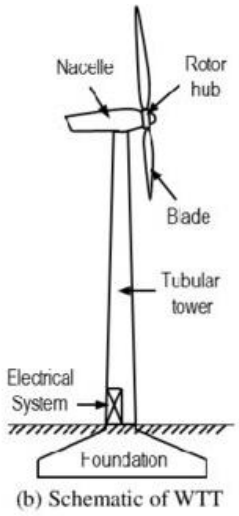

Figure 2: Schematic of wind turbine assembly [34]

A typical wind turbine assembly consists of a concrete foundation, a steel or copper tower and a nacelle attached to three blades, as shown in figure (2). However, the blades are mainly manufactured using composite materials i.e. glass fibers and some plywood inserts. The use of composites in manufacturing the wind blades make recycling them a difficult challenge. In fact, thermoset matrix-based composite disposal is one of the most difficult environmental

challenges because of the “cured” nature of composite materials, which refers to the cross-linking phenomena that occurs between the polymeric chains in the “curing” process.

Including work on wind turbine blades, the extensive literature has discussed several methods for recycling glass fiber thermoset composites. Unfortunately, the proposed recycling methods failed to establish a well-defined practice with high commercialization capacity. Furthermore, the wind energy sector is relatively young in such a way that there is a lack of experience on blade recycling. More concerns will arise as more materials are generated with growth of the wind energy sector. One study that was done to define the materials used in manufacturing the blades showed that 75% of the wind turbine blade weight consists of composites [35]. In general, vacuum-assisted resin transfer molding (VARTM) is the main process used to manufacture the blades by infusion with a high-grade epoxy or polyester [36].

Figure 3: Disposed/ landfilled wind blades [37-38]

There is no doubt that the materials and production methods will evolve in the future. Some case studies predict that carbon fiber will be used more increasingly in future designs, causing further environmental effects [39]. Nevertheless, the current situation does not provide a clear

sight of this transformation since the high price of carbon fiber and carbon processability keep changing.

Consequently, some attempts have been performed on the environmental aspects of wind energy precisely on the waste volume of wind turbine blades. 1.18 million tonnes volume of waste is estimated in 2017 compared to 260,000 tonnes in 2008. Moreover, it has been projected that for every 1KW of electricity generated by the wind sector, there is 10kg of wind turbine blade material that will be used, such that 1MW corresponds to 1 tonne of blade material [40]. Fifty thousand tonnes of blade waste per year was projected to be produced by the end of the current year with a projection that the number will be more than 200,000 tonnes by 2034 [41].

With the evolution in wind turbine blade size accompanied by the rapid transformation of world energy supplies to more sustainable sources, more waste is predicted to be generated in the next decades. As mentioned earlier, it has been estimated that for each 1KW of electricity, there will be a 10kg of material that should be reused or recycled [41]. In another study, it is estimated that 400,000 tonnes of waste per year will be produced between 2029 and 2034 [42]. Likewise, 800,000 tonnes of waste material per year will be available for recycling by 2050. However, the previous studies failed to consider the growth of wind turbine sizes over the next decades, which will make the estimation less representative of futuristic waste volume. It must be mentioned that the wind energy industry will keep developing progressively both in scope and in technology and generating more material that will need to be recycled [11].

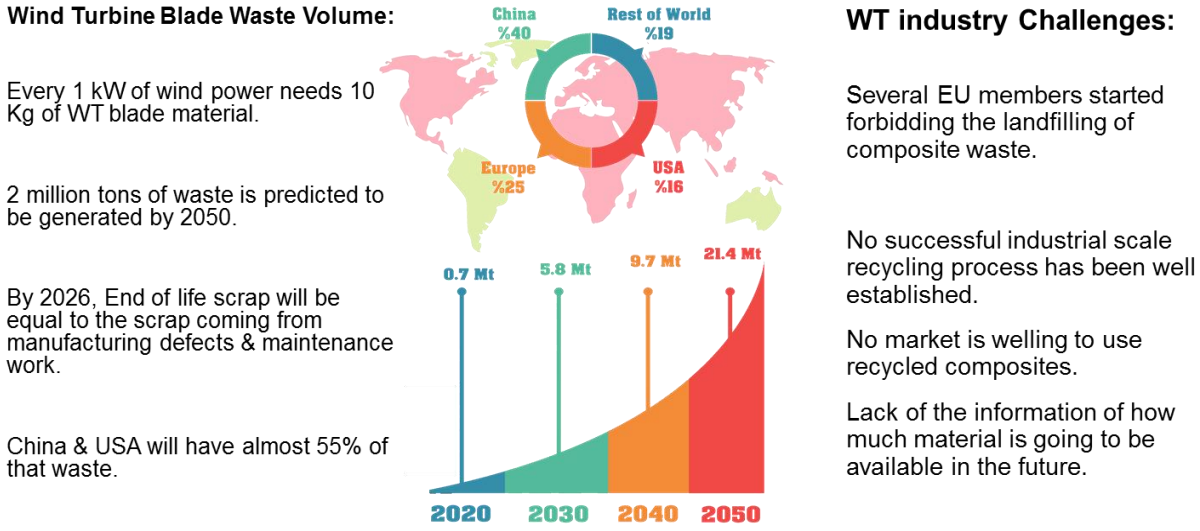

Figure 4: Total WTB waste in the next three decades with the geographical distribution around the world [10-13]

Clearly, the massive amount of end-of-life WT blades needs an adequate solution to deal with this ever-increasing problem. More comprehensive studies, including the change of blade size and geographical effects, predict a higher amount of waste generated in the future compared to previous studies. Some researchers have provided an estimate of total waste while considering the change of blade size and lifecycle contributing factors [39-41]. However, a full study quantifies the total wind turbine blade waste, which includes end-of-life, manufacturing, and service waste, which will exceed 21.4 Mt within the next three decades. It also showed that 2Mt annual waste would be generated and disposed by 2050 raising real concerns by governments and environmental groups [11]. With more waste being generated, there should be more sustainable practices and methodologies for dealing with wind turbine blade recyclability issues and that should be accompanied by more strict governmental regulations. These restrictions on fiberglass waste are already in place in countries like Germany and France, and will likely be in place in North America in the next few years.

2.3. Recycling Overview

The eclectic nature of composite materials makes them challenging to be recycled. In fact, the thermoset polymers that are used to bond the fibers together, can not be remolded or melted due to their cross-linked micro-composition nature, as shown in figure (5). Polymeric chains in thermoset polymers are attached by covalent bonds, which make them insolvent, unrecyclable nor soluble [42].

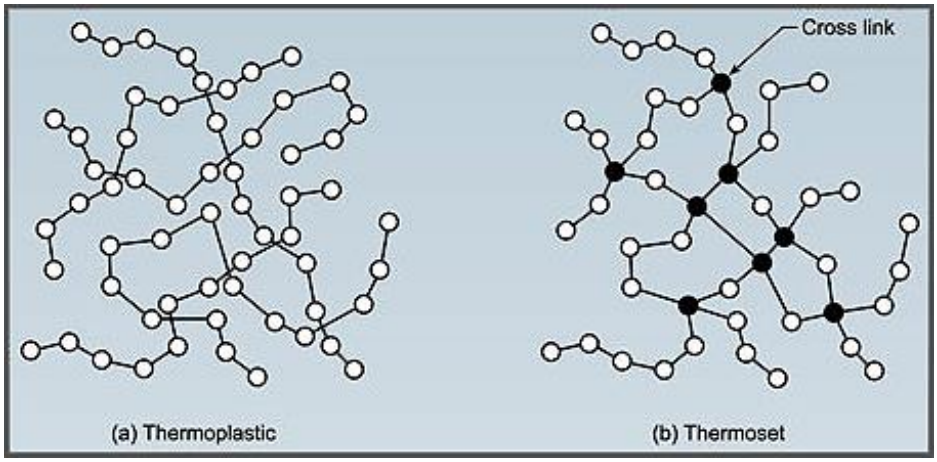

Figure 5: The difference between thermoplastic and thermoset polymers [42]

Governments and major wind turbine manufacturers currently do not have comprehensive data about future blade waste volume. However, they still alert that end-of-life waste needs to be addressed soon. As discussed earlier, waste generated from the wind energy sector is likely to grow rapidly within the next three decades reaching massive volumes and unfortunately, all the proposed recycling methods have failed to establish well-defined recycling practices with high commercialization capacities.

Landfill and incineration are the most common routes commonly used to dispose of wind turbine blades. In fact, landfilling blades would lead to a major source of dangerous and harmful blade materials that might seep into the ground and poison the water table. Furthermore, the inorganic ingredients result in the release of toxic flue gases, so that the tiny glass fiber sparse creates problems for dust filter devices.

While landfill is obviously not environmentally friendly, incineration is also the mainstream route proposed in the literature to deal with wind turbine blade waste. This gives an advantage over landfills, because 60% of the scrap is toxic due to the synthetic compounds used in composites manufacturing. Incineration is a thermal oxidation process, which is burning the material to create heat. It is considered as a heat recovery process rather than material recycling, which recovers the energy stored in the organic material. Ash is the main output and it is usually disposed to landfills [43].

Figure 6: The landfilling of blades [44]

Recently, the recycling of wind turbine blades has been considerably investigated in the literature to resolve landfill, incineration, and other issues. The recycling processes can be categorized into three main categories: thermal, chemical and mechanical [45]. All processes are well-discussed in the literature with extensive work being developing in each of the three categories.

2.3.1. Mechanical Recycling

First, Mechanical recycling starts with a low-speed cutting process reducing the blades to suitable smaller-sized pieces that will be easier in handling and transporting the scrap and removal of any inserts as well. In a second step, these pieces are hammer-milled or ground to smaller pieces that are 0.05mm to 10mm in size.

Finally, the recyclate is separated into different fractions i.e. fiber-rich (coarser) and matrix-rich (finer) recyclate fractions [46]. Sorting via sequential sieves, hydro-cyclone sorting, electrostatic sorting, near-infrared, optical sorting and flotation sorting are the main typical classification methods found in the literature [47-49]. One study showed that the potential applications of recyclate are limited as a result of their lower mechanical properties. The results showed that the recyclate fibers feature lower tensile strength compared to virgin fibers and poor interfacial strength between the polyester matrix and the recyclate fibers was observed as well. The quality of the fibers' surface is the reason for weakening the interfacial properties, which prevents good bonding between the matrix and the fibers. Nevertheless, mechanical recycling is considered to be the only mature and environmentally friendly process found in the current market [50-51].

2.3.2. Thermal Recycling

Thermal recycling methods are mainly used to recover pure solid residues that are the reinforcing fibers. This is in contrast to mechanical recycling where reclaimed fibers can be still attached to some of the matrix material. Thermal processes heat composites at high temperatures in order to breakdown the material into constituents like gas, liquid and solid chars (residues left behind by the thermal process) [52]. The main thermal recycling methods are fluidized-bed combustion and pyrolysis.

2.3.2.1. Fluidised-Bed Combustion Recycling Process

This method is effective in recycling thermoset composites with several constituents. While this method is capable of reclaiming fibers, it is incapable of reclaiming different valuable products from the breakdown of the thermoset matrix, i.e., monomers that could be reused as a raw material supplies in other industries [53]. In order to recover the fibers and fillers, the size of the scrap is reduced to 25mm sized pieces, on average, and then they are fed into a closed chamber with circulating hot air that heats a fluidized silica sand bed as shown in figure (7).

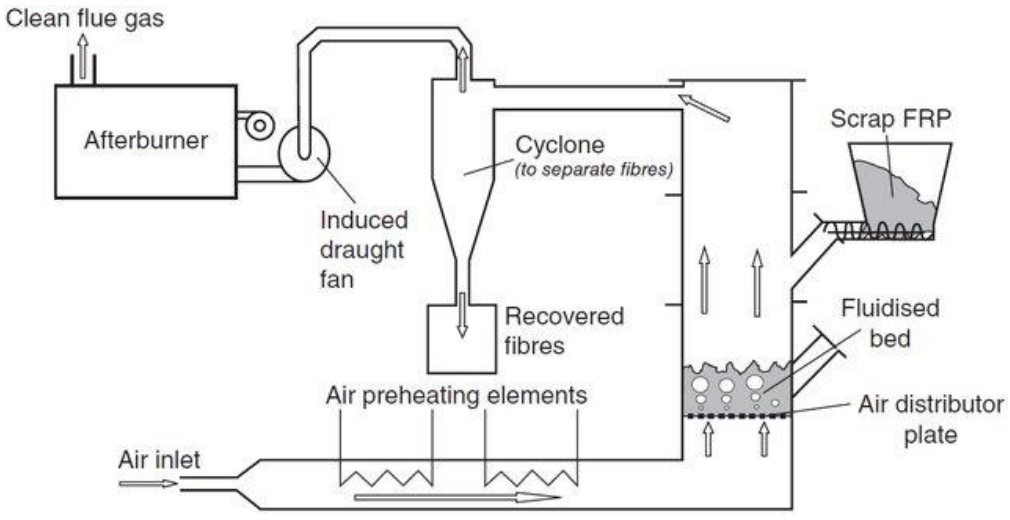

Figure 7: Fluidized bed process scheme [54]

Electric preheating elements are used to heat the air up to the 400–550°C temperature range. Then, air is distributed while passing an air distributor plate attached to the bottom of the silica sand bed. At this stage, the scrap is being fed into the bed and the passing air will cause a bubbling regime that will ensure a uniform temperature distribution in the bed. The temperature of the fluidized bed is selected to be high enough to decompose the polymer. However, it should not be extremely high to avoid a partial degradation of the fibers. Air temperature of 450°C has been found to be suitable for polyester resins, where epoxies tend to need higher temperatures due to their higher thermal stability [55]. Fluidized bed is useful for the recovery of both carbon fiber and glass fibers.

As a result of the high temperature of the bed, the polymer breaks down and volatilises from the composite in the range of temperatures between 450-550°C. Finally, a secondary combustion process is performed to fully dissolve the polymer by oxidation and purify the recovered fiber and filler particles [56]. Some studies performed on the mechanical properties of the recycled fibers showed that the reclaimed fibers suffer from a 25% drop in the tensile strength. The final form of the recovered fibers is generally in a fluffy mat with surface conditions similar to virgin fibers. Moreover, the recovered fibers outlined in the literature thus showed degradation in their mechanical properties. Pickering showed in two studies that a 50% drop in the compressive strength of fluidized bed processed SMC fibers [32, 52].

2.3.2.2. Pyrolysis Process

Even though the pyrolysis process has been used now for many decades with carbonaceous materials, it is considered a non-conventional method for recycling synthetic polymers. In contrast to fluidized bed process, pyrolysis is a thermochemical degradation

process of a material in the absence of oxygen, causing a depolymerization of the thermoset matrix which result in the formation of small organic substances that involve carbon solid char, liquid and non-condensable gases [57].

It is quite useful for recovering reinforcing fibers with relatively high mechanical properties. Pyrolysis is performed in the absence of oxygen to limit the probability of any chemical reactions that could affect the mechanical performance of the reclaimed fibers. Moreover, the captured gas and liquid resulting from decomposed polymer can be re-used as a supply in several applications [56]. A char layer will be generated from polymer breakdown and it will cover the surface of the fibers resulting in lower surface quality. In fact, an oxidative isothermal process usually follows the pyrolysis leading to the dissolving of chars.

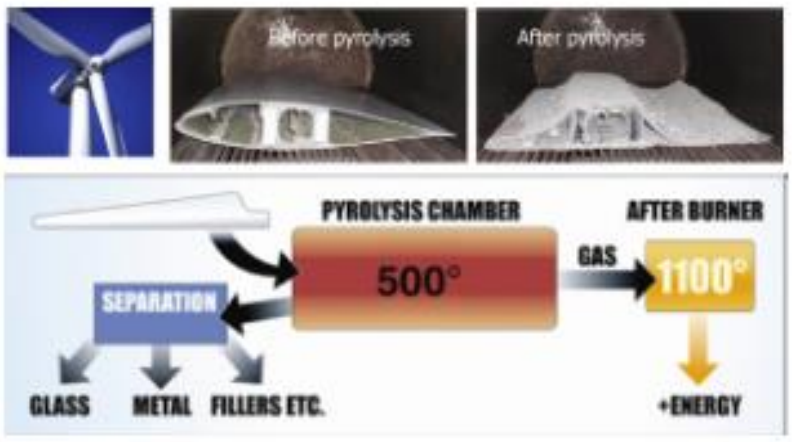

Figure 8: The pyrolysis processing scheme [58]

Epoxies, vinyl esters and polyesters are the main typical matrix materials used to make thermoset composites. Due to the strong bonds of cross-linked polymeric chains, higher temperatures are needed to decompose the matrix. In a recent study, Cunlie [59] found 50-60%

tensile strength drop in recycled fiberglass recovered from oriented circuit boards by pyrolyzing and dissolving the polymer [59]. Nevertheless, pyrolysis is considered one of the most effective and capable technologies for recycling thermoset composites with minimum effect on the quality of the reclaimed fibers.

2.3.3. Chemical Recycling

Several chemical techniques have been recently developed investigating the ability to depolymerize thermoset resins in order to be able to separate the fibers. Recently, polymer chemical recycling has received significant consideration [60]. The thermoset matrix is decomposed using a chemical dissolvent agent. The polymer is broken down into high-value oligomers. In other words, resins dissolve after the depolymerization process and inorganic substances such as metals inserts, glass fiber (GF) and carbon fiber (CF) can be recovered. The dissolution process can be very reliable, depending on the type of the solvent used and the process parameters like temperature and pressure [61]. For example, when water or alcohol is used as a solvent, high temperature and pressure are generally required, under either sub- or supercritical conditions. A supercritical fluid is a state where substance behaves like a gas. This makes the depolymerization process easier and results in faster dissolution and greater efficiency [62].

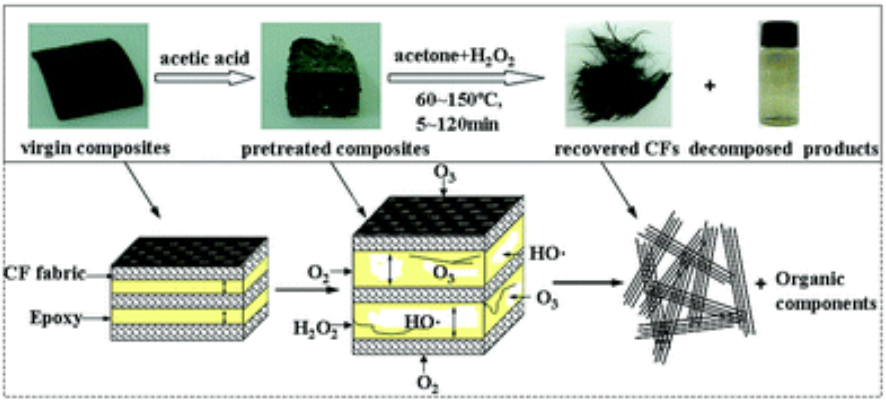

Figure 9: The hydrolysis process as an example of chemical recycling [63]

Due to its excellent processability and crosslinked nature, epoxy resin is considered a great candidate for several composite applications. In terms of recycling epoxy, several studies showed the low resistivity of epoxy in acidic medium at high temperature resulting in the possibility of complete matrix removal using some acidic agents [64]. These studies are promising finding as possible solutions to the recyclability issue of epoxy composites. However, despite the efficiency of separating fibers, the extensive use of dangerous chemicals and unnecessary prolonged methods limits the possibility of scaling these methods to an industrial commercialization level. The resulting dangerous waste chemicals negate the whole purpose of finding a sustainable recycling solution.

2.4. Additive Manufacturing

Additive manufacturing (AM) refers to any processes that involve "adding" material layer-by-layer to form a new 3-Dimensional object. AM technologies have made it possible to produce vast and diverse models that are too complex to be manufactured by conventional methods [65]. Stereolithography (SLA), laminated object manufacturing (LOM) and Fused

deposition modeling (FDM), are the main AM techniques available in the market [66-68]. SLA uses photopolymerization to create a solid 3D object by cross-linking the polymers. In more detail, a vat of photopolymer resin is solidified by focusing an ultraviolet laser that creates the shape layer-by-layer according to computer-aided design (CAD). SLA is frequently used to make 3D plastic or resin structures and can also be used for tissue engineering applications with soft materials like hydrogels [67].

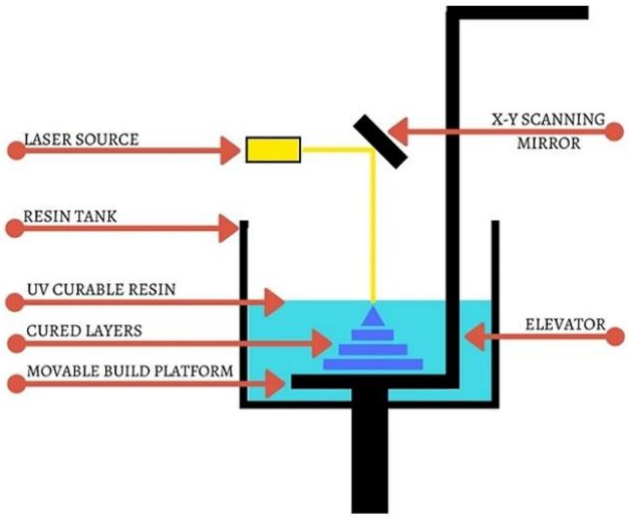

Figure 10: Stereolithography [69]

FDM is considered the most widely used process for manufacturing pure plastic parts at low prices. FDM is 3D printing method that is accomplished by depositing a melted layer of a thermoplastic filament using a moving depositing nozzle to create an object. A thermoplastic filament is heated by a printer head that is capable of melting the filament to create a structure from the bottom upwards. The printer nozzle moves back and forth accordingly to the STL file, adding layer over layer until completion of the desired structure. The most commonly used materials in FDM are thermoplastic polymers, i.e., Polylactic Acid (PLA), Acrylonitrile Butadiene

Styrene (ABS) and polyurethane. A pre-fabricated filament spool is loaded to the machine in the process, as shown in figure (11). Once the nozzle reaches the specified temperature, i.e., close to the polymer's melting temperature, the filament is fed into the extrusion head, then into the nozzle. In general, FDM 3D printing is used to develop experimental prototypes with relatively low mechanical properties [65]. Therefore, the development of stronger thermoplastic parts produced by FDM is important because it will enhance their usability and capabilities. One way to address this issue is to apply reinforcement materials like glass fibers to thermoplastic materials to produce a glass fiber reinforced 3D printing filament.

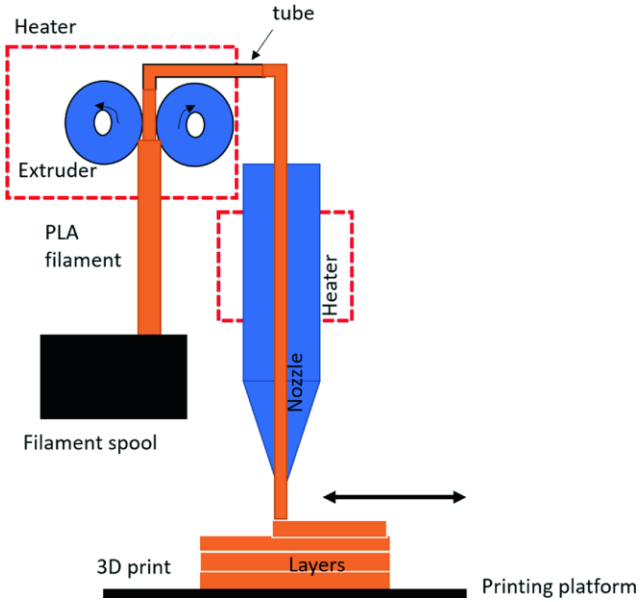

Figure 11: Fused deposition Modelling FDM [70]

Many works in the literature investigated the possibility of incorporating short and long fibers within thermoplastics for making FDM filaments. Halil investigated the processability, microstructure and mechanical performance of ABS samples reinforced with 0.2-0.4mm (chopped Hexcel AS4) carbon fibers [71]. He found that the tensile strength and modulus of 3D-

printed samples increased by 115% and 700%, respectively. In another detailed study carried out on the effect of nozzle temperature, infill speed and layer thickness effects on the mechanical performance of carbon fiber/ABS composites were studied. It has been shown that, at higher nozzle temperature and infill speeds, lower tensile strengths were observed [72].

The capability resulting from the use of glass fibers in reinforcing ABS matrix was studied by Farahikia. He showed that glass fibers could improve the tensile strength and stiffness of the ABS filaments. In another study, Gray developed a new filament made from polypropylene (pp) composites reinforced by thermotropic liquid crystalline polymer (TLCP) fibers [73]. They reported that filament with longer TLCP fibers had higher tensile strength compared to filament with the chopped fibers. However, both resulted in more strength and improved prototype functionality than without TLCP reinforcement. Moreover, Shofner reported 40% and 60% enhancement in tensile strength and young modulus, respectively, in ABS filament made from single-walled carbon nanotubes [74].

2.5. Theoretical Modelling of Composite Tensile Properties

In general, the variation of fibre lengths and their orientations results in more complexity in predicting the strength and Young's modulus for discontinuous fibre composites compared to aligned continuous fibre composites. Mainly, the shearing mechanism, which is at the fibre/matrix interface, is responsible for transferring the applied tensile load via the matrix between the reinforcing fibres. The matrix usually has a longitudinal strain that is higher than the reinforcing fibres and by assuming an ideal bond between the two constituents, the longitudinal strain difference will create a shear stress distribution across the fibre/matrix interface as shown in figure (12). Also, by neglecting the stress transfer at the fibre end cross-

sections and the interaction between the neighboring fibres, the normal stress distribution in a single fibre can be calculated as follows, by considering an infinitesimal cylindrical object with length dx located a distance x from one fibre end, the equilibrium equation can be written as:

$$\left(\frac{\pi}{4}d_f^2\right)(\sigma_f + d\sigma_f) - \left(\frac{\pi}{4}d_f^2\right)\sigma_f - (\pi d_f\, d_x)\tau = 0 \quad (1)$$

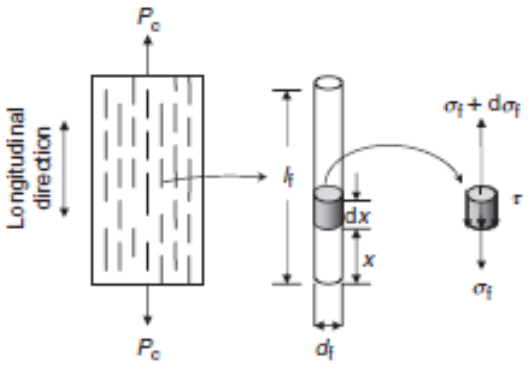

Figure 12: The equilibrium FBD of infinitesimal cylindrical volume [75]

And by doing some simplifications:

$$\left(\frac{d\sigma_f}{dx}\right) = \left(\frac{4\tau}{d_f}\right), \quad (2)$$

where,

σ_f: fibre longitudinal stress a distance x from one of the ends.

τ: shear stress at the fibre/matrix interface.

d_f: fibre diameter.

By recalling the assumption of no stress transfer at fibre ends, $\sigma_f = 0\ at\ x = 0, L$, and by integrating equation (2), the fibre stress distribution can be written as,

$$\sigma_f = \left(\frac{4}{d_f}\right)\int_0^x \tau\, dx. \tag{2*}$$

and by assuming a constant shear stress τ_i,

$$\sigma_f = \frac{4\tau_i}{d_f}x \tag{3}$$

The fibre stress is not uniform in a composite lamina containing discontinuous fibres. Precisely, it is equal to zero at fibre's end and it increases linearly reaching maximum value as we approach the middle sections of the fibre. The maximum stress occurs at the center of the fibre and it can be calculated at a given load by:

$$(\sigma_f)_{max} = 2\,\tau_i\frac{l_t}{d_f} \tag{4}$$

where x = $\frac{l_t}{2}$, which is known as the load transfer length from the fibre end. Thus, l_t is the minimum length required to achieve the maximum fibre stress for known fibre diameter and fibre/matrix interfacial strength. The critical length l_c can be calculated using the following equation:

$$l_c = \frac{\sigma_{fu}}{2\tau_i}d_f \tag{5}$$

σ_{fu}: ultimate tensile strength of the fibre.

τ_i: shear stress at the fibre/matrix interface.

l_c: critical length, the minimum length required in order to achieve maximum stress at a given load.

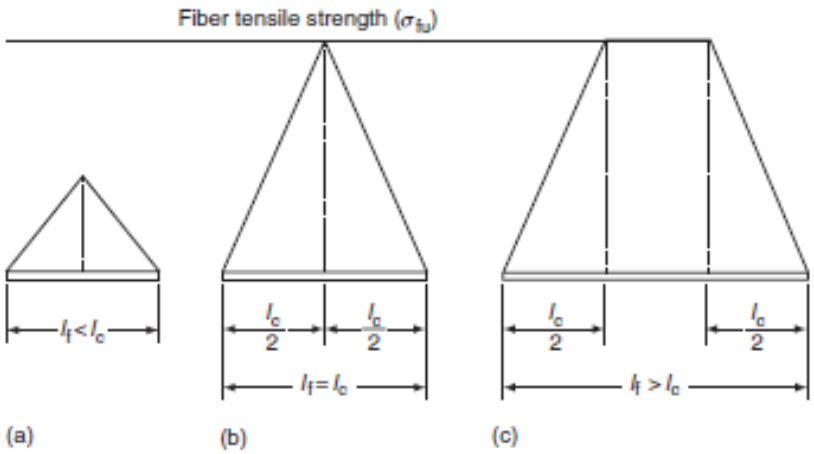

Figure 13: Stress distribution within the fibre based on x-distance from one fibre end [75]

Based on the length of the reinforcement fibres, several failure mechanisms can be observed:

- For $l_f < l_c$, the maximum fibre stress will never reach the potential fibre strength. In this case, the fibre–matrix interface will fail first before any fibre reaches its ultimate strength. The average tensile stress in the fibres can be written as a function of interfacial strength and the aspect ratio of the fibres $\overline{\sigma}_f = \tau_i \frac{l_f}{d_f}$. The composite longitudinal strength can be calculated using the following equation:

$$\sigma_{Ltu} = \tau_i \frac{l_f}{d_f} v_f + \sigma_{mu}(1 - v_f) \quad (6)$$

where σ_{mu}: matrix ultimate tensile strength.

- For l_f > l_c , the maximum fibre stress reaches the ultimate fibre strength. Moreover, over a distance equal to l_c / 2 from each end, the fibre remains less effective as shown in figure (13). The longitudinal tensile strength of a unidirectional discontinuous fibre composite is calculated by equation (6a):

$$\sigma_{Ltu} = \sigma_{fu}(1 - \frac{l_c}{2l_f})v_f + \acute{\sigma}_{mu}(1 - v_f) \quad (6a)$$

where,

$\acute{\sigma}_{mu}$: matrix tensile strength at the fibre failure strain.

σ_{fu}: is the tensile strength of the fibre.

The value of l_c can be controlled by the value of τ_i for a given fibre diameter and strength. For example, using a coupling agent could boost the τ_i value, which will lower the required value of l_c. Also, l_c can be reduced by applying a proper fibre surface treatment. In other words, increasing reinforcement effectiveness can be obtained without the need to use longer fibres. The volume fractions of fibre and matrix are noted by v_f and v_m which can be found using equations (7a-7b):

$$v_f = \left(\frac{V_f}{V_f + V_m}\right) \quad (7)$$

$$v_f = \left(\frac{\frac{m_f}{\rho_f}}{\frac{m_f}{\rho_f} + \frac{m_m}{\rho_m}}\right) \quad (7a)$$

$$v_m = (1 - v_f) \tag{7b}$$

where, v, m and ρ are the volume fraction, mass and the density, respectively, while f and m subscripts represent the fibre and matrix.

2.5.1. Rule of Mixtures Model (Parallel)

The Rule of Mixtures (RoM) is one of the most popular models to predict the longitudinal and the upper and lower limits for strength and stiffness of unidirectional continuous fibre composites. With an iso-strain condition, which neglects the difference in fibre and matrix individual strains, RoM is considered to be the simplest prediction model available. The format is a direct summation of different weighting of individual constituent properties by their volume fraction. It should be noted that this model assumes a perfect interfacial bonding between the fibre and the matrix [75-77]. According to this model, Young's modulus and strength can be found using the following equations:

Longitudinal direction:

$$\sigma_c = \sigma_f v_f + \sigma_m v_m \tag{8}$$

$$E_c = E_f v_f + E_m v_m \tag{9}$$

where, E, σ and v are Young's modulus, strength and volume fraction, respectively, while the subscripts c, f and m are referring to composite, fibre and matrix, respectively. Even though the model has demonstrated to have a good approximation for predicting composite properties, it should be noted that porosity content is assumed to be equal to zero. Besides the effect of lowering the composite load bearing volume, porosity affects the composite mechanical

properties by introducing stress concentrations into the material. A further theoretical study was done by MacKenzie [78] on porosity effects on the tensile properties of the composite. He quantified the effect by adding spherical holes into the geometry and introduced an approximation which can be calculated using:

$$X_P = X_d(1 - v_P)^2 \tag{10}$$

where p and d denote the porous and the fully dense geometries, respectively, while X could be E or σ. The following equations are the modified rule of mixture models for short fibres reinforced composites with porosity effect considered:

Longitudinal direction:

$$\sigma_c = (\sigma_f v_f + \sigma_m v_m)(1 - v_P)^2 \tag{10a}$$

$$E_c = (E_f v_f + E_m v_m)(1 - v_P)^2 \tag{10b}$$

2.5.2. Halpin Tsai

This model has been used extensively for modelling and predicting the properties of short fibre reinforced composites in a wide range of applications. Due its semi-empirical nature, it can give a very accurate estimation of the mechanical response of several mixtures. This model was first introduced in 1969 by Halpin and Tsai and it was mainly proposed to a specific context [75-79]. Subsequently, extensive work done was performed by other researchers to extend and to widen the scope of the model. The semi-empirical nature of this model can be applied to predict the tensile strength and Young's modulus of aligned discontinuous fibre

reinforced composites, resulting in more precise predictions compared to the Rule of Mixtures model [79].

Longitudinal direction:

$$E_L = \frac{1 + 2(\frac{l_f}{d_f})\eta_L v_f}{1 - \eta_L v_f} E_m \tag{11}$$

$$\sigma_L = \frac{1 + 2(\frac{l_f}{d_f})\eta_L^* v_f}{1 - \eta_L^* v_f} \sigma_m \tag{12}$$

where,

$$\eta_L = \frac{\left(\frac{E_f}{E_m}\right) - 1}{\left(\frac{E_f}{E_m}\right) + \zeta} \tag{11a}$$

$$\eta_T^* = \frac{\left(\frac{\sigma_f}{\sigma_m}\right) - 1}{\left(\frac{\sigma_f}{\sigma_m}\right) + \zeta} \tag{12a}$$

where, $\eta_T \; and \; \eta_T^*$, are two geometrical factors that take into account the relation between the mechanical properties of the constituents, and ζ, which is a shape fitting parameter that is

usually given by $\zeta = \frac{2l}{d}$, or 2, for the transverse direction. L and d are the average values of fibre length and diameter, respectively.

Fibre aspect ratio is defined as the fibres' average length l_f divided by fibres' average diameter d_f. $E_L \; and \; E_T$ are derived from the Halpin-Tsai equations and they are valid under the following conditions:

- Fibre cross section is circular.
- Fibres are arranged in square arrays.
- Fibres are uniformly dispersed throughout the matrix.
- Perfect bonding at fibre/matrix interface.
- Matrix is free of voids.

However, for the second assumption of the fibre arrangement, further work has been done by Nielsen by introducing factor ψ which considers the different arrangement-packing shapes, enabling a better estimation:

$$E_L = \frac{1 + 2(\frac{l_f}{d_f})\eta_L v_f}{1 - \eta_L \psi v_f} E_m \tag{11*}$$

$$\psi = 1 + \left[\frac{1 - \theta_{max}}{\theta_{max}^2}\right] v_f \tag{11*a}$$

where θ_{max}, is the maximum packing fraction of the fibres for a specific fibre arrangement, which is equal to 0.907, 0.785, 0.82 for hexagonal, square and random fibres arrangements, respectively [18].

2.5.3. Cox Model

The Cox model is one of the earliest models adopted to predict the tensile strength and Young's modulus of discontinuous aligned reinforced composites. Like the Halpin-Tsai model, this model assumes the existence of a perfect bond at the fibre/matrix interface. Shear lag theory is the backbone of the development of this model, which assumes stress transfers to fibres by shearing load introduced at the fibre/matrix interface. Both the matrix and the fibre are assumed to be elastic and isotropic. In general, shear stress reaches the maximum at the fibre ends and decreases reaching zero at the fibre centre [79-80]. For shorter fibres, fibre failure does not occur. In this instance, debonding would be expected, which will lead to fibre pull-out during composite failure.

$$\sigma_c = \sigma_f v_f \left[1 - \frac{tanh(\frac{\beta l_f}{2})}{\frac{\beta l_f}{2}}\right] + \sigma_m v_m \tag{13}$$

$$E_c = E_f v_f \left[1 - \frac{tanh(\frac{\beta l_f}{2})}{\frac{\beta l_f}{2}}\right] + E_m v_m \tag{14}$$

$$\beta = \sqrt{\frac{2G_m}{E_f r_f^2 \ln(\frac{R}{r_f})}} \tag{15}$$

The value of reinforcement effectiveness reduction factor $\left[1-\frac{tanh(\frac{\beta l_f}{2})}{\frac{\beta l_f}{2}}\right]$ approaches unity if $\frac{\beta l_f}{2}$ is large enough, which brings the model back to the simple Rule of Mixtures model, but if $\frac{\beta l_f}{2}$ is small, it tends to zero.

$$R_{hexagonal} = \sqrt{\frac{2\pi r^2}{\sqrt{3}v_f}} \tag{15a}$$

$$R_{square} = r\sqrt{\frac{\pi}{4v_f}} \tag{15b}$$

Summary

The above-mentioned theoretical models will be evaluated and used in comparison with experimental results to be presented in the following section.

3. Experimental Method

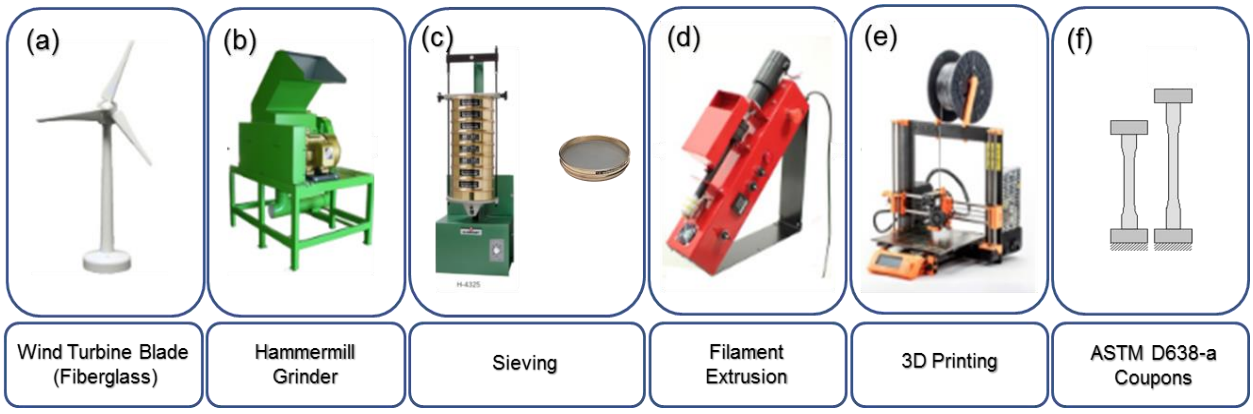

Figure 14: Process cycle scheme (a) wind turbine blade, (b) mechanical grinding, (c) sieving, (d) filament extrusion, (e) 3D printing resting coupons and (f) mechanical testing

3.1. Mechanical recycling

Due to its high-volume yield, versatility, low energy requirement and small environmental footprint, mechanical recycling is the best choice for this project, compared to other recycling methods. It can be defined as a size reduction process by applying a mechanical force, i.e., shredding, grinding and/or crushing. In general, mechanical recycling does not generate any waste or any harmful chemical materials during the process. Moreover, it is considered to be the only method widely used in industry so far compared to other methods that are still at the laboratory scale [81]. Nevertheless, the final yield is a mix of fibers and resin in the form of powder, which lowers the final market value of the fibers.

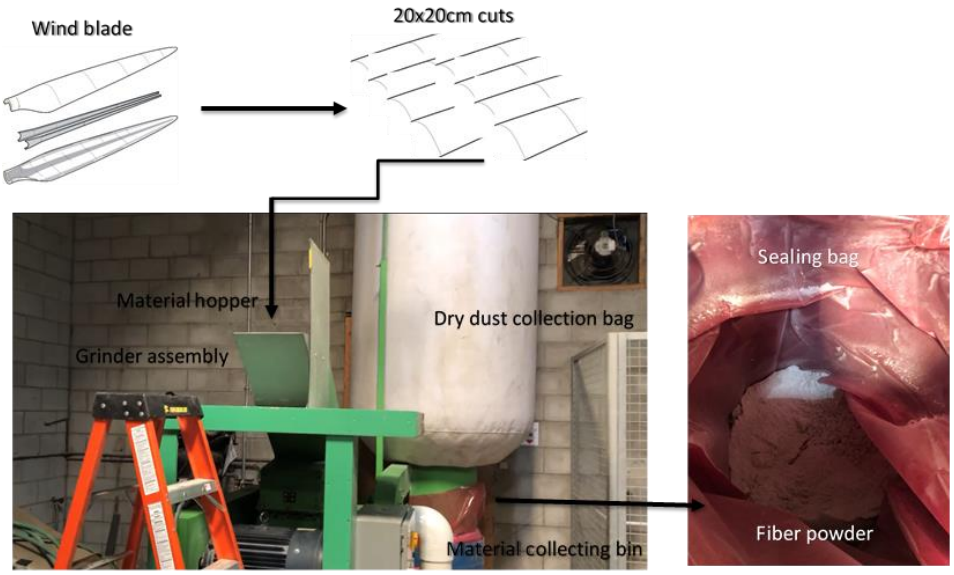

Figure 15: Grinder assembly (left) and the final ground wind turbine blade material (right) [Eco-wolf]

In this study, mechanical recycling is used to convert reinforced wind turbine blades into reduced-size fibers/resin powder. Firstly, 20 × 20cm parts are cut from bigger blade sections that do not include any core materials. Secondly, these parts are fed into a hammer mill grinder (ECO-WOLF, INC., Edgewater, FL, USA) breaking the pieces down into fibers/resin powder that is collected in a sealed bag. A visual inspection reveals that the final mixture has a combination of short and long glass fibers as well as resin particles and powder. A photo of the grinder and collector is shown in figure (15).

3.2. Sieving and Separation

Sieving is an essential process to separate the grinder output (recyclate) into different size grades. In this study, the process is performed using a Humboldt, Economy Sieve Shaker with 8'' diameter multi-level sieves (figure 16). The sieves are stacked on the top of the cradle

frame by placing the finest sieve at the bottom followed by increasingly coarser sieves with the coarsest being on top. Then, the recyclate batch is loaded to the top sieve and covered and secured using the attachment screws. The shaker applies a vibration to promote the separation. The duration of each run is 30 minutes to fully separate the material.

Figure 16: Humboldt, Economy Sieve Shaker (left) with 8" Dia., No. 140 (106µm) Brass Frame Stainless Mesh (right) [82]

The lowest sieve has openings at the smallest range, which restricts it to particles that are less than 0.4 mm in diameter. This size is equal to the 3D printer nozzle diameter ensuring that no-blockage can occur later on when these particles are used in the FDM 3D printing process. Even with multiple and/or prolonged sieving runs, used to ensure the effectiveness of the separation process, there are still some long fibers found in the finest sieved material.

3.3. Fiber length and diameter characterization

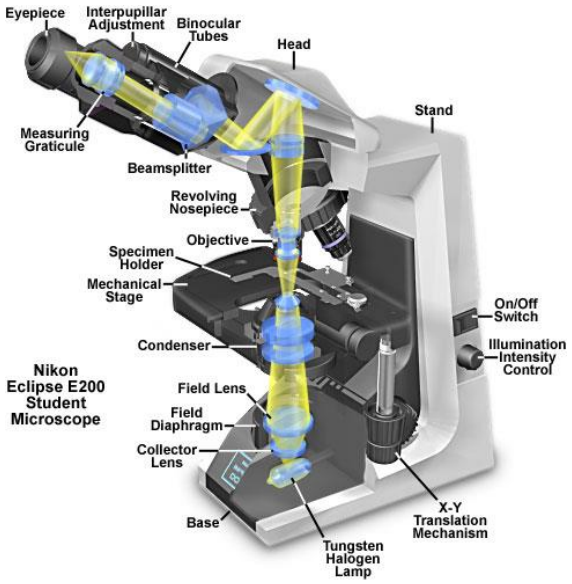

Figure 17: Nikon e200 microscope, details of its components, used in the visual inspection [83]

After the repeated sieving process, the material from the final sieve was characterized to define the aspect ratio of the reclaimed fibers of this sieve. Firstly, 10 random samples were taken from the sieved material, to remove any bias in the results. Subsequently, they were placed on (FisherbrandTM) plain microscopic glass slides and they were visually observed and recorded using an (Nikon-e200) optical microscope as seen in figure (17). 10µm magnification power was sufficient to capture and show both short and long fibers in a single picture.

In total, 465 ground fibers were observed under the microscope and their associated lengths and diameters were documented and sorted using Dijimizer software. A statistical distribution and normality test were performed on the data collected using (MinTab2017) software to identify the existence of distinct groups within the reclaimed material. In other

words, having more than one peak in the generated histogram will indicate more than one distinct fiber group is used in the manufacturing of the wind blades.

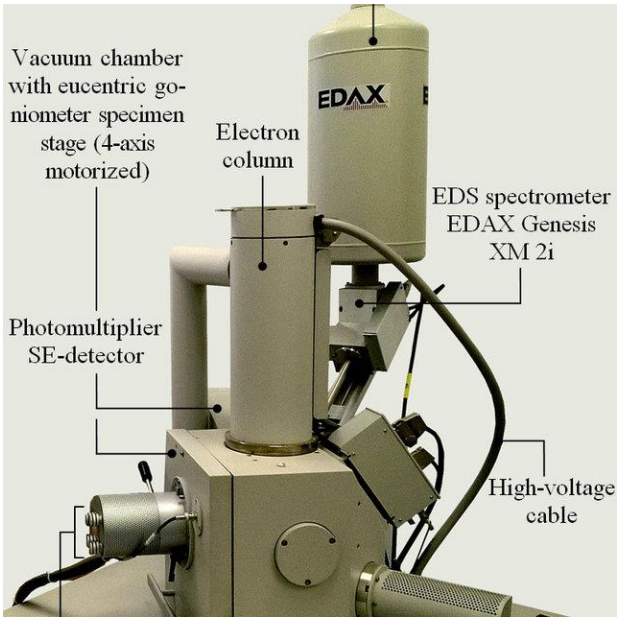

Figure 18: General view of scanning electron microscope components [Wojciech 2018]

Additionally, the surface morphologies of the different fiber batches, i.e., virgin, ground, and pyrolyzed fibers, were examined using a (Hitachi UHR Cold-Emission FE-SEM SU8000) scanning electron microscope. The process started with mounting fibers on aluminum pin stubs. Then, a 6nm platinum layer was applied to coat the fibers in order to get more refined pictures. Finally, fiber surfaces micrographs were recorded using a (5k accelerating voltage) secondary electron detector placed in a vacuum chamber. The fiber micrographs for the different fiber batches are reported and summarized in the results section.

3.4. Fibre Weight Fraction and Degradation Temperature Analysis

Thermalgravimetric analysis (TGA) is a thermal-analytical method where a sample mass is monitored over time while the temperature is changing. This analysis is carried out by a device usually called thermogravimetric analyzer which has a precision balance attached to a pan located inside a furnace with a programmable control temperature. TGA is considered to be a convenient analysis method to define certain information regarding certain aspects of material behaviour, namely: mass change, oxidative and thermal stability, and material constituent's breakdown [84-85].

This analysis offers direct indication of polymer thermal breakdown temperature and purity. Usually, controlling parameters like purge gas flow rate, temperature and atmosphere gases are used to fully characterize different material behaviour under different conditions. Figure (19) shows a typical TGA graph for Polylactic PLA plastic.

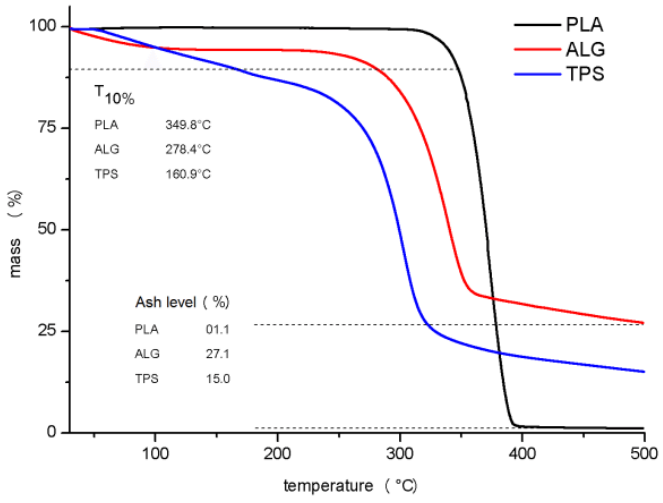

Figure 19: TGA graph for PLA %mass vs. temperature [84]

Thermogravimetric analysis (TGA) was performed to characterize the recycled materials. This analysis was conducted to find the total amount of epoxy residue within the recycled material. Several replicate samples with weight ranging between 10 to 23 mg were used from the different sieved materials to quantify the proportions of fiber and epoxy within the different sieving grades. In this study, the tests are first performed using the Q500 from TA Instruments, (New Castle, DE, USA) and then the results are analyzed using TA universal analysis software.

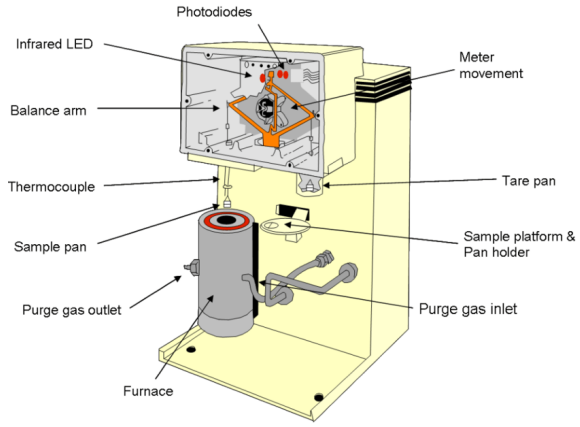

Figure 20: Schematic of TA Q500 TGA Download Scientific Diagram [85]

The samples were heated to 550^{o}C at a heating rate of 25 °C/min. All runs were carried out in a nitrogen atmosphere to limit the chemical reactions that can occur during the process. Subsequently, the remaining material was held at 550^{o}C for 20 min to guarantee a full decomposition of the char layer that was produced during epoxy molecular chain breakdown during the first temperature ramp. The main goal of performing the tests was to find the proportions of epoxy within the recyclate. Moreover, another goal was to define the lowest

temperature needed to fully decompose the epoxy residues, which will be used later in the pyrolysis study on one fiber batch.

3.5. Recyclate Thermolysis

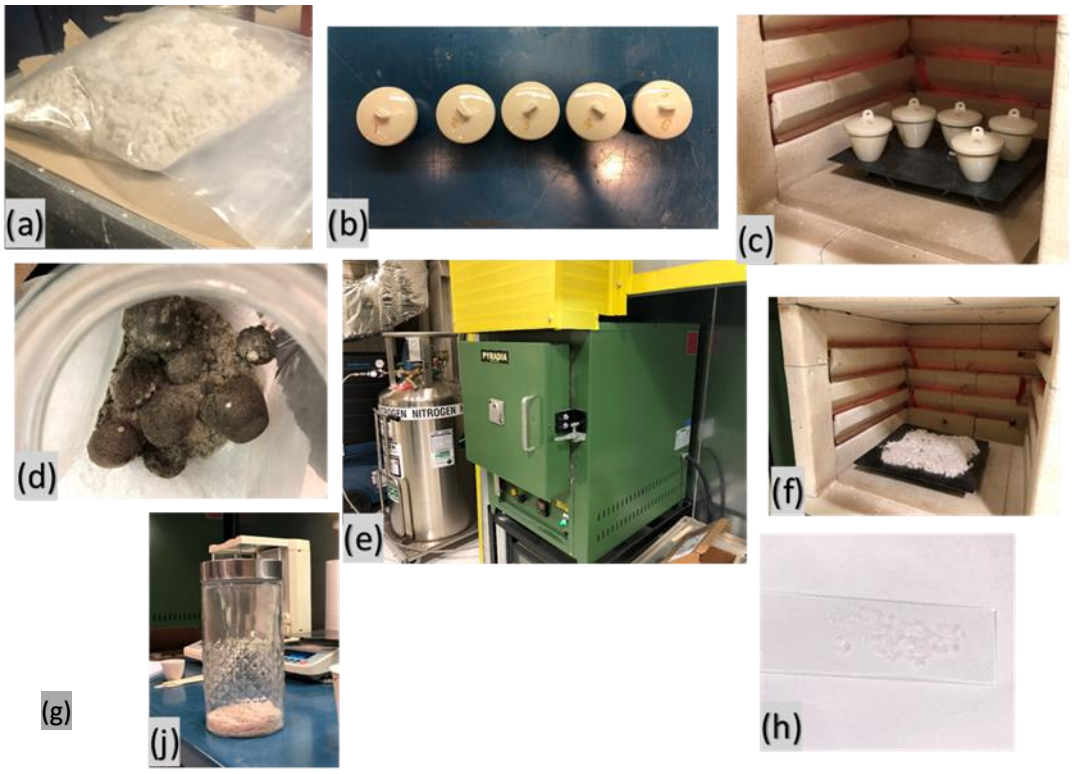

Figure 21: Pyrolysis steps: ground fiber sample (a), distributed fibers in small ceramic crucibles (b), placing them in the furnace (c), pyrolyzed fibers with char layer (d), pyrolysis oven (e), fibers after the oxidative stage (f), reclaimed samples after the thermolysis process (g, h).

The crosslinking behaviour of the thermoset matrix molecules is the main challenge since the material can not be remolded or re-melted. Unlike mechanical recycling of thermoset composites, which generates a mixture of fiber and resin powder, thermolysis processes, e.g., pyrolysis and fluidized bed are more applicable to separate the different constituents efficiently and isolate the fibers.

In this study, 400g of the sieved ground fibers were pyrolyzed using the F200 PYRADIA, Quebec, Canada furnace. Firstly, the samples were distributed into 10 (Eisco Labs) ceramic crucibles that were placed inside the furnace, as shown in figure (21). With a nitrogen atmosphere, these crucibles were maintained at 550°C for 45min. Finally, an isothermal oxidative stage at the same temperature for 15min was used to remove the char layer resulting from resin breakdown found on the surface of the pyrolyzed fibers.

Furthermore, to perform the single fiber tensile and pull-out tests, some long individual fibers were separated from the ground and pyrolyzed fiber bundles which were taken from the unsieved recyclate, as shown in figure (22).

Figure 22: Bundles of long fibers: ground fibers (a), pyrolyzed fibers (b)

3.6. Single Fibre Tensile Test

In the present work, the Tensile Strength and Young's Modulus for High-Modulus Single-Filament Materials (ASTM-D3379-75) test procedure was performed to measure fiber tensile properties. The specimen preparation started by isolating a thin single fiber from a bundle of fibers, which required a tremendous effort. After that, each fiber end was glued into a plastic tab, as shown in figure (23).

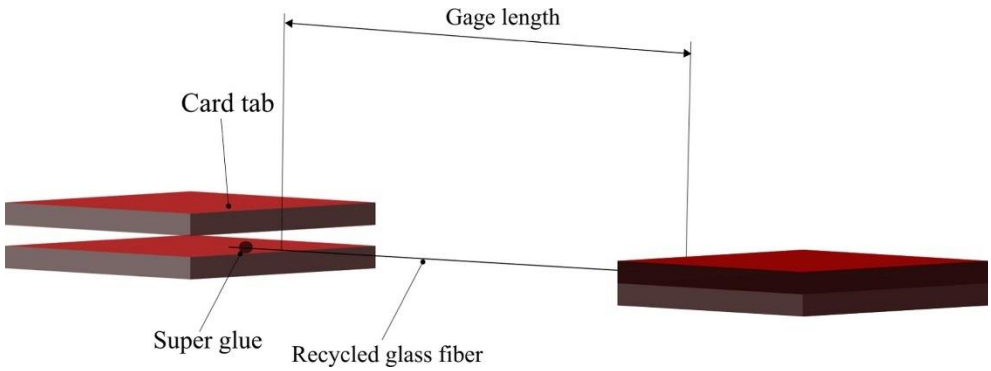

Figure 23: Single fiber tensile test specimen preparation [90]

Then, the samples were loaded into a 10N-load-cell (Instron Model 3342 universal testing machine) to perform the test at a loading rate equal to 0.1 mm/s. A special extensometer was used to capture the extension of the fiber. The load was applied gradually to the fiber failure load. Load vs. displacement curves were recorded and the data was extracted and analyzed. The stress vs. strain graphs and strength, stiffness and failure strain results are presented in the results section.

Figure 24: Instron Model-3342 universal testing machine

3.7. Single Fibre Pull-Out Test

The fiber/matrix interface has a critical effect on the mechanical properties of composites. Although there are many tests used to characterize the interface, like single fiber pull-out, single fiber fragmentation and fiber push-out tests, thus far it remains a difficult challenge to characterize the interface for a couple of reasons.

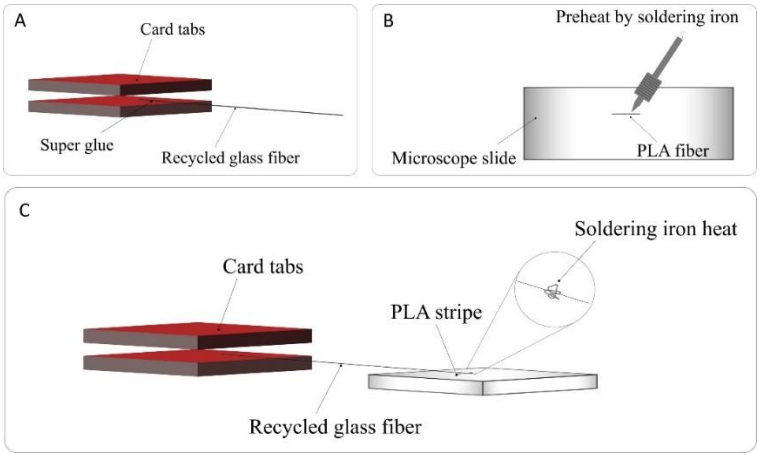

Figure 25: Single fiber pull-out test sample preparation [90]

The primary challenge was the separating and handling of single fibers with the naked eye, without special equipment. Secondly, in some cases the fiber will fail before the interface, which is defeating the objective of the test. Moreover, mounting samples in the testing machine required a lot of caution so as not to break the very fragile fibers. Finally, the test needs special devices, i.e., a 10N load cell and a powerful extensometer to be able to capture those small extensions. In this study, specimens were first prepared by gluing one fiber end to a plastic gripping tab. Then, the single PLA fiber was attached to a transparent glass tab where free fiber end was embedded in a bead of resin, as shown in figure (25). Then, the samples were loaded using a 10N load cell (Instron Model 3342 universal testing machine) and the test was performed at a loading rate equal to 0.1 mm/s. The load was applied gradually so that the failure would occur at the fiber-resin interface. Load vs. displacement curves were recorded and the data was extracted and analyzed.

Both single fiber tension tests and single fiber pull-out tests are presented in the fourth section.

3.8. Filament Extrusion Process

One critical parameter contributing to the final performance and governing the mechanical properties of a composite is the fiber dispersion within the matrix. Firstly, fibers and PLA (Ingeo 4043D, Natureworks LLC, Blair, NE, USA) were mixed carefully in 1:3, 1:5 and 1:10 ratios to extrude filaments with 3%, 5% and 10% reinforcement content, respectively. To achieve adequate fiber distribution, a double extrusion process was performed using an (Leistritz ZSE18HP-40D, Nuremberg, Germany) extruder with 8 sub-temperature-zones.

The temperature profile is summarized in table (1). The process started with pouring the mixed materials into the hopper. Then, two rotating screws enclosed in a stationary heated barrel were used to mix the PLA molten pellets with fibers. After that, the mixture was drawn through a 1.75mm diameter die and the extrudate was then cooled using a water bath to solidify it. Finally, the filament was cut into small pellets that will be used in another extrusion step. Figure (26) shows the scheme of the process showing the different components.

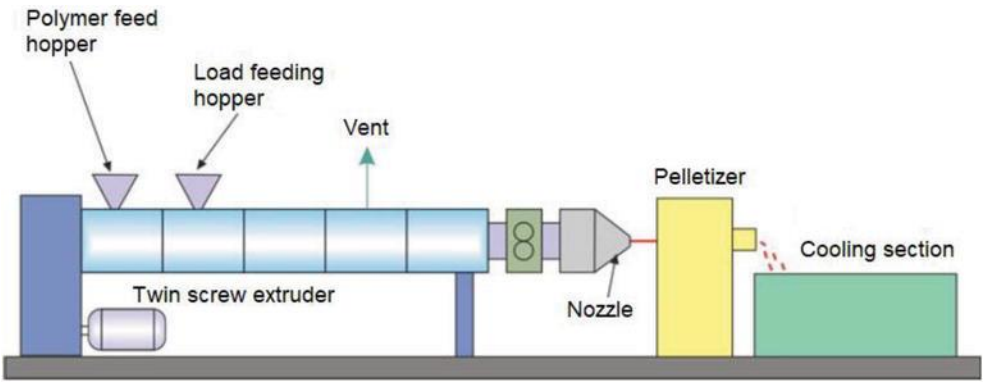

Figure 26: Extrusion process scheme [86]

Table 1: Extruder temperature profile

Extrusion Screw speed (rpm)	90
Subzone 1–2 (Temp °C)	190
Subzone 3 (Temp °C)	185
Subzone 4 (Temp °C)	180
Subzone 5 (Temp °C)	175
Subzone 6–8 (Temp °C)	170

Using the pellets from the previous step, a single screw extrusion process was performed using the (FilaFab PRO 350 EX, Bristol, United Kingdom) extruder to manufacture the final printing filaments. While the extrudate was continuously being drawn through 1.75mm die and solidifying using air, a ±2µm accuracy laser micrometer was used to monitor the variation of the filament diameter. The extrusion parameters are summarized in table (2).

Table 2: Single screw extrusion parameters

Auger speed (rpm)	25
Die temperature (°C)	210
Winder Speed (rpm)	1

3.9. Reinforced Coupons Tensile Test

ASTM D638-a is the most well-known standard for tensile property assessment for reinforced polymers. In this study, the objective is to compare the influence of the different reinforcements used, i.e., virgin, ground and pyrolyzed fibers, as well as their content effect (Weight fraction) on the tensile properties of the composite. A 50kN 313Q tensile machine (TestResources) was used to test the prepared specimens with a displacement rate equal to 5 mm/min. The specimens were loaded, and load was applied gradually while the coupon extension was being measured by an attached extensometer.

Load vs. displacement data points were recorded by the machine software. Subsequently, (FE-SEM SU8000 Cold-Emission, Hitachi, Ltd, Japan) a scanning electron microscope was used to study the fracture surface. Both stress vs. strain graphs and microscopic images of the fracture surfaces are presented and discussed in the results section.

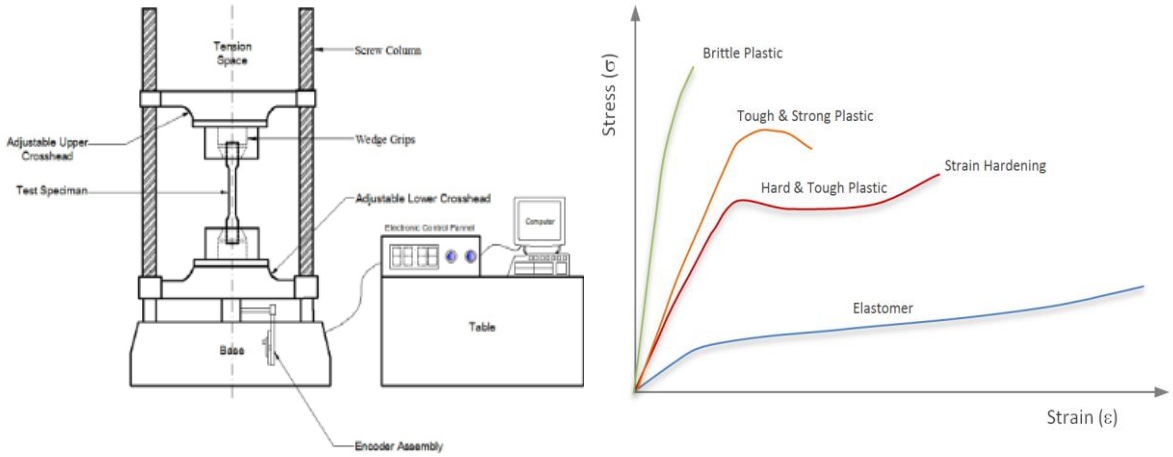

Figure 27: Tensile test schematic (left) and typical stress vs. strain graphs for different polymer types (right) [87].

4. Results & Discussion

4.1. Summary of Previous Work

Previous studies showed the effect of the fiber content on the mechanical tensile performance of 3D printed coupons [88-89]. Testing samples were manufactured with different fiber content, i.e., 5%, 10%, 15%, 20% and 25%. Subsequently, a 50kN 313Q tensile machine (TestResources) was used to perform the tests on the prepared specimens with a displacement rate equal to 5mm/min. The specimens were loaded, and load was increased gradually while the extension was being measured by an attached extensometer. Load vs. displacement data points were recorded by the machine software. Typical stress vs. strain curves for the tested coupons are presented in figure (29).

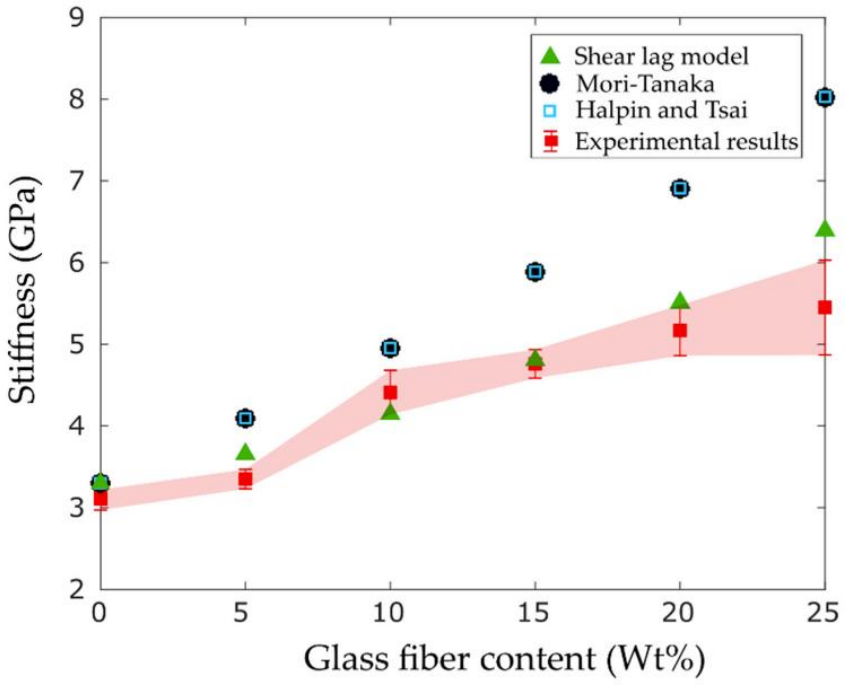

Figure 28:Stiffness experimental results with some predicted models [89]

Correspondingly, an increase in fiber content led to an increase in the mean tensile stiffness of the samples. There was a major improvement in the stiffness from 5%Wt_f percent to 10%Wt_f percent. A 74% improvement was observed for 25%Wt_f percent of fiber content. In addition, pure PLA samples exhibited the highest failure strain of 2% while 25%Wt_f composite samples had the lowest mean strain failure, equal to 0.7%, which represents a 65% reduction. A significant drop in tensile strength was observed in the reinforced coupons. The findings reveal that, as the fiber content increases, the average tensile strength of the samples decreases whereas a reduction of 42% is reported for specimens of 25%Wt_f.

Table 3: Experimental results vs the predicted models (Mori-Tanaka, Halpin-Tsai)

Longitudinal Young Modulus GPa			
%Weight Fraction	Halpin-Tsai	Mori-Tanaka	Experimental results
0	3.2	3.2	3.1
5	4.03	4.05	3.2
10	5.1	5.1	4.1
15	5.8	5.85	4.2
20	7.2	7.16	4.9
25	8	8	5.1

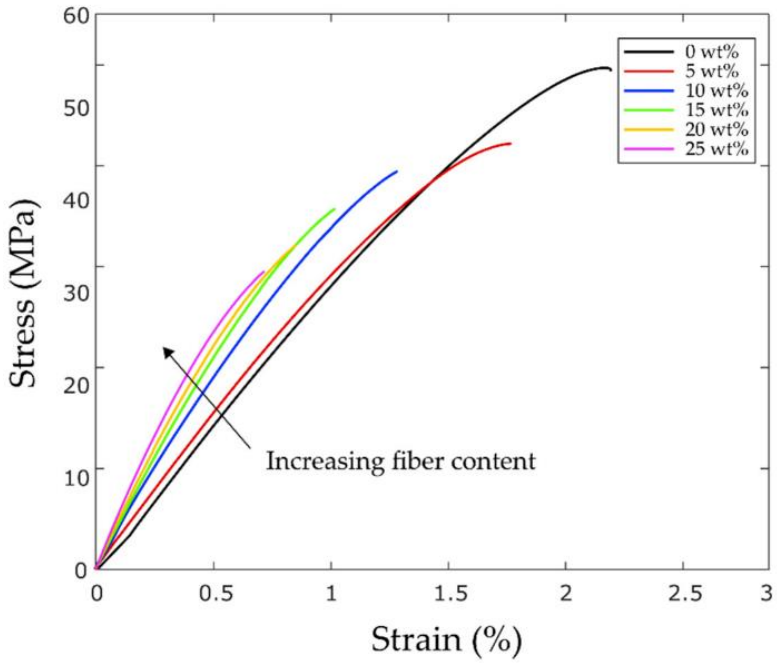

Figure 29: Stress vs strain curves for the tested specimens [89]

Table 4: Strength values vs reinforcement percentage

Strength MPa	
%Weight Fraction	Experimental Results
0	50
5	45
10	38
15	36
20	33
25	30

The various developed analytical models, including the Halpin–Tsai, shear lag model and the Mori–Tanaka equations were used to model and compare the elasticity modulus of short glass fiber composites to the tested printed parts. The predictive models exhibited a similar pattern to the experimental measurements and were in good agreement, especially at the lower weight fractions. Nevertheless, the high viscosity of the polymer at higher weight fiber fraction combined with the blockage of the nozzle significantly increased the porosity of the 3D printed parts, leading to a higher difference between the experimental results and the predicted values, according to [89].

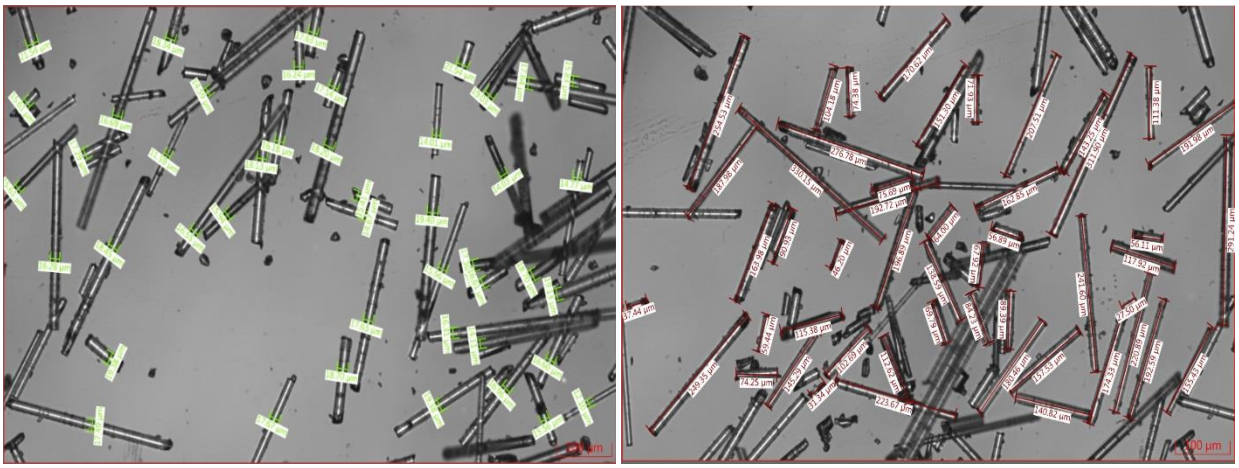

Figure 30: Samples of fiber length and diameter calculations

4.2. Micromechanical Models

In order to fully develop the micromechanical models, four main parameters should be defined first. The fibre/matrix tensile properties (σ_f, σ_m, E_f, E_m), aspect ratio (l_f/d_f), interfacial strength (τ_{IFSS}) and the fibre weight fraction ($\%Wt_f$) are the initial parameters needed to establish the models.

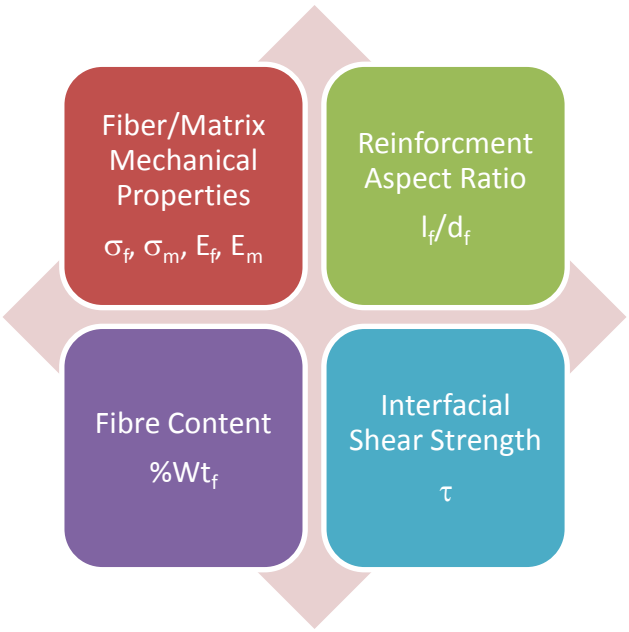

Figure 31: the four initial parameters needed to establish the prediction models.

4.2.1. Aspect Ratio AR (l_f, d_f):

In the earlier work, the aspect ratio (length of fibers divided by their diameter) is reported to be equivalent to 5.8, by taking the mean of 100 inspected random fibers using a microscope. In this study, to verify the actual aspect ratio, yet more characterization of the length and diameter of the fibers was carried out.

465 random fibers were investigated using (Nikon e200) microscope with a magnification power equal to 100X characterise the length and diameter of the fibers. Typical samples of fiber microscopic images are shown in figure (30). The range of fiber lengths was found to be between 27.5-537.9µm and diameters between 10.6-22.5µm. The microscopic images have been analysed using (Dijimizer software). The lengths and diameters of the fibers were documented and exported to a separate excel sheet.

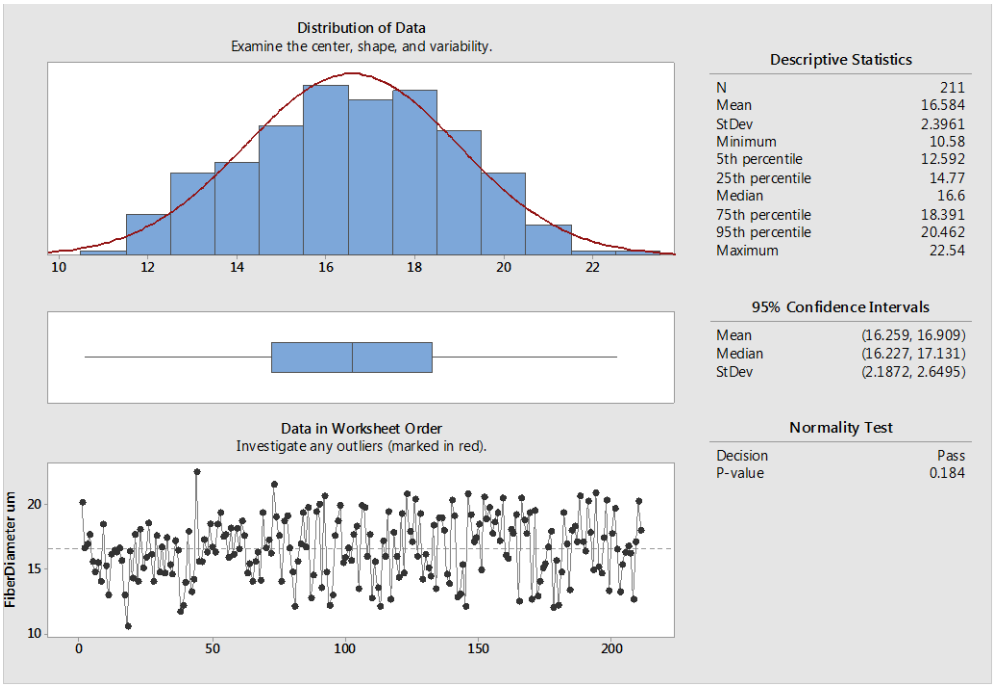

Figure 32: Fiber diameter distribution

From the data collected using (MinTab2017) software, a statistical distribution and normality test was carried out. Firstly, a histogram for the diameters of fibers was generated to represent their distribution graphically. As shown in figure (32), a symmetrical bell curve about the mean is depicted, thus a normal distribution. For normal distribution, 68% of the observations are within $\mu \pm \sigma$ while 95% are $\mu \pm 2\sigma$, and 99.7% are $\mu \pm 3\sigma$ for a normal distribution. The diameters mean and standard deviation are equal to 16.6 $\pm$2.4µm. 68% of fiber diameters are between 14.77-18.39µm.

Minitab software is further used to check the distribution of fiber lengths and their histogram is introduced in figure (33). The normality test was performed using the software and it reveals that fiber lengths are not normally distributed. This is due to the fact that the last,

smallest sieve size still allows some long fibers to pass through by means of their small diameters.

However, a Weibull distribution was fitted to the data with 255.7 and 2.078 as the scale and shape parameters, respectively. The small value of the shape parameter indicated the amount of scattering of the data. The mean value was found to be 226.1µm while the standard deviation is equal to 115.4µm.

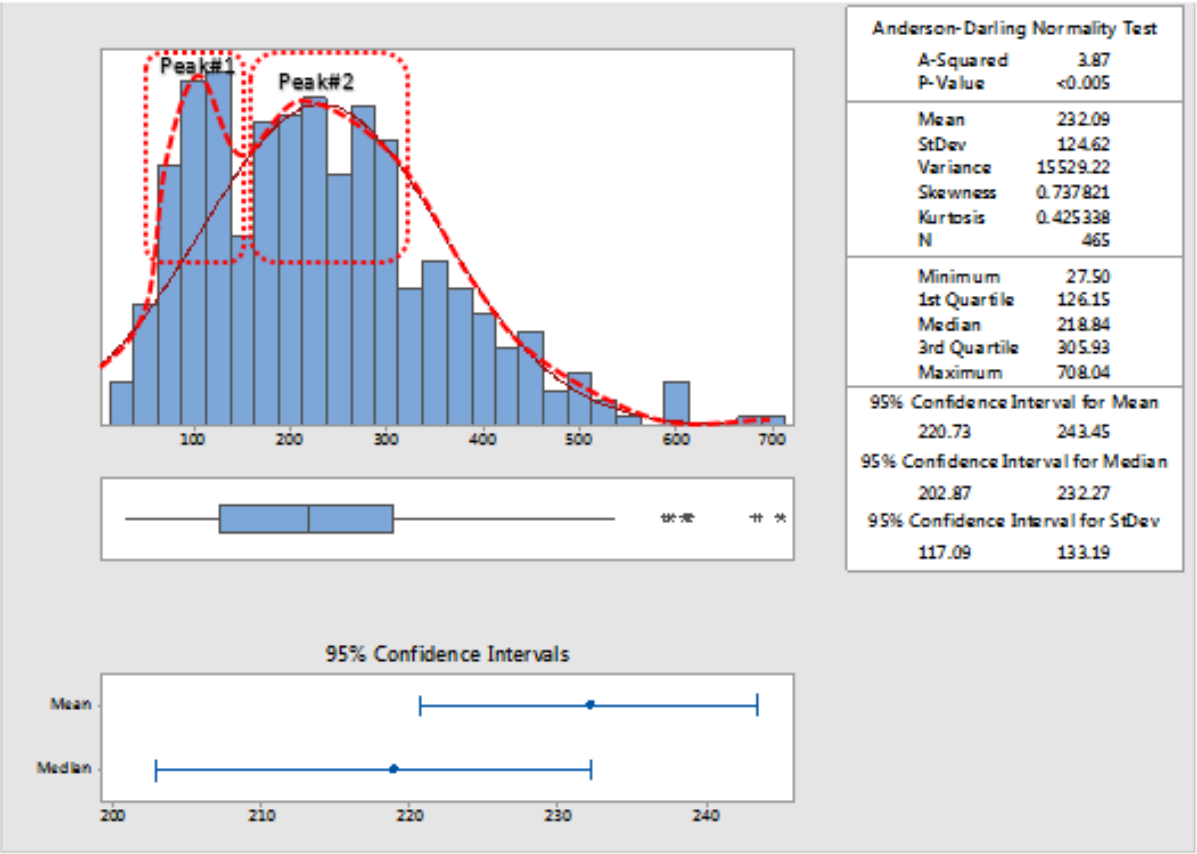

Figure 33: Fiber length distribution

The distribution of fiber lengths is shown in figure (33). 68% of Fiber lengths are within the 125.61-301.8µm range. Both fiber length and diameter distribution parameters, i.e., mean,

standard deviation, confidence intervals (CI) are reported in table (5). Aspect ratios based on the mean values and the CI boundaries are summarized in table (6). The aspect ratio is almost 2.5 higher than the reported value in a previous study, which has an important influence on the results from the theoretical models [89].

Table 5: Reported old and modified mean fiber length and diameter

Parameter	Length μm	Diameter μm
Average	226.1	16.6
Standard Deviation	124.6	2.4
Median	218.8	16.6
95% CL upper limit	301.8	18.4
95% CL lower limit	125.6	14.8

Table 6: Reported old and modified aspect ratios

Aspect Ratio (l/d)	
$l_{average}/d_{average}$	13.62
l_{max}/d_{min}	20.39
l_{min}/d_{max}	6.82
l_{old}/d_{old}	5.88

4.2.2. TGA Results $\%Wt_f$

Thermogravimetric analysis and derivative thermogravimetry were carried out simultaneous using a TGA thermal analyzer device (TA instrument Q500). The samples (13–

24mg) were placed in a platinum pan and heated up to 650°C at a rate of 20°C/min under nitrogen purge (50 mL/min). The mass loss as a function of temperature followed the traditional sigmoid-like shape. As the scanning temperature increased to 380°C, a dramatic decline was observed corresponding to epoxy decomposition.

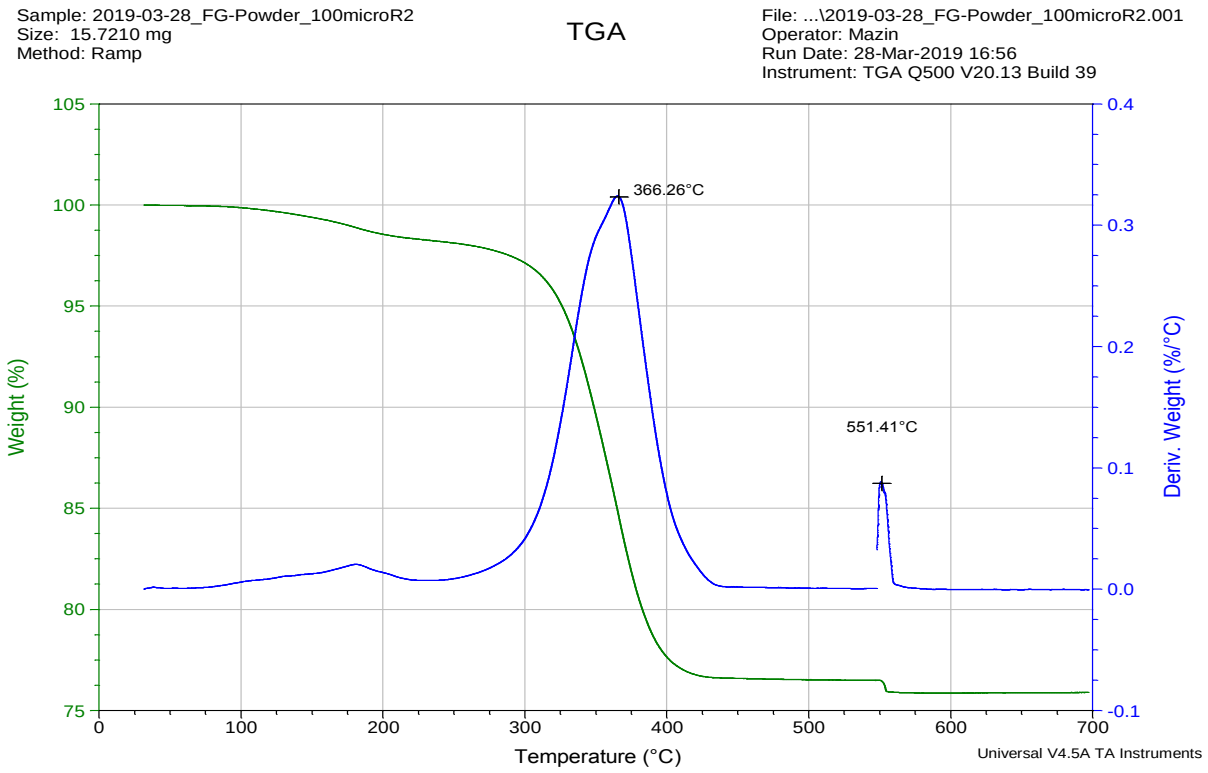

Figure 34: TGA graph of recyclate (Sieved ground powder)

Like a previous study [90], sieved ground fiber showed two distinct stages of breakdown: During the first stage (225–410°C), a total weight loss equal to 23.8% occurred, representing the loss of epoxy particles. Further, a 1.5% small weight loss was observed between (510-525°C), which is attributed to the decomposition of the solid char that was generated from epoxy breakdown. It should be noted that nitrogen was used in the first phase

of the analysis (20-500°C) while oxygen was used after in order to decompose the ash layer at a temperature equal to 551°C. The total weight remaining after the analysis was 77.5% ± 3%, which represents the solid glass fibers, as shown in figure (36).

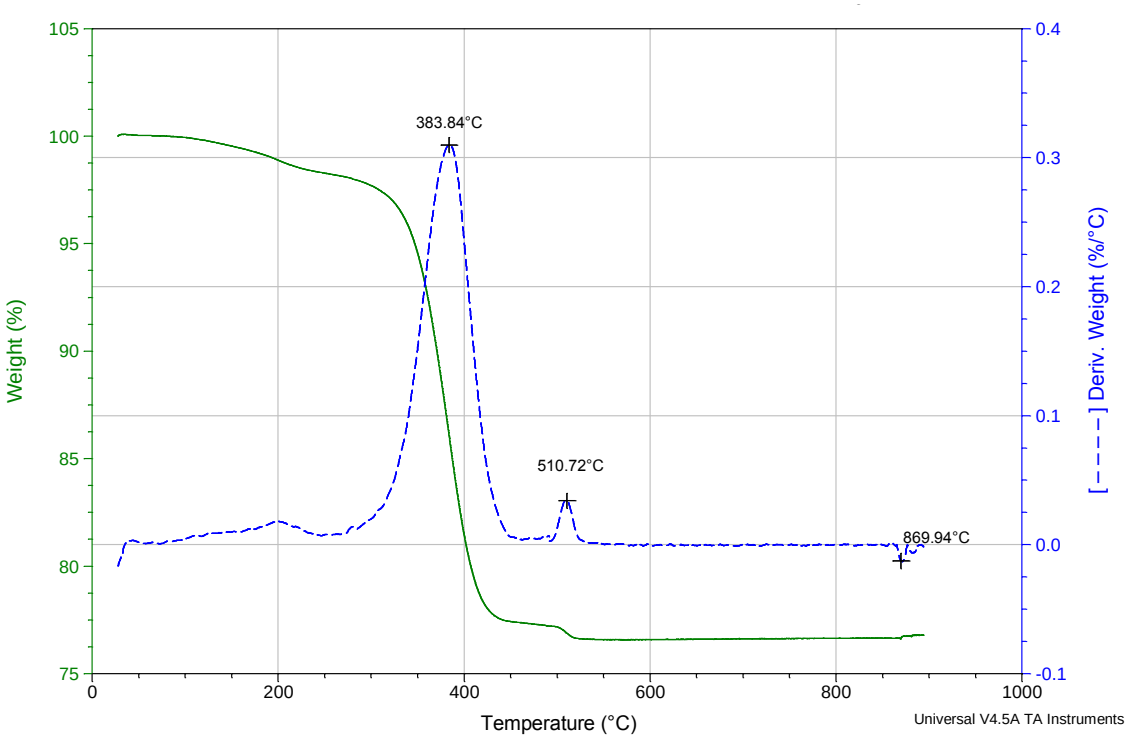

Figure 35: TGA graph of recyclate (Sieved ground powder) until temperature of 900°C

One sample was heated to 900°C at a rate of 20°C/min and a small peak was detected in the DTG graph around 869°C, which was not captured in the other runs. A microscopic image of the tested fibers revealed distorted fiber geometry, i.e., cylindrical shape, as shown on the right in figure (36).

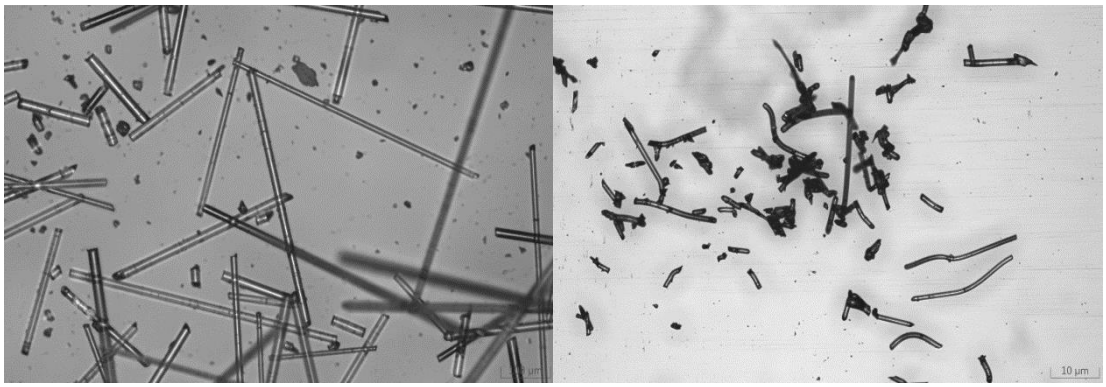

Figure 36: Comparison between fibers from the TGA runs, 900°C (right), 650°C (left)

A further analysis was carried out on the extruded filaments to define the fiber weight fractions and to check the effectiveness of the double extrusion process in maintaining the defined mix ratios. In other words, the PLA pellets and recycled fibers were mixed in specific ratios 3%, 5% and 10% of reinforcing filaments, respectively. In fact, mixing ratios are expected to have some variation from the set target. Thus, the predictable composite tensile properties will have some variation from the target values due to that inefficiency. The TGA curves for all different fiber types and content are shown in figure (37) for the ground, pyrolyzed and virgin fibers.

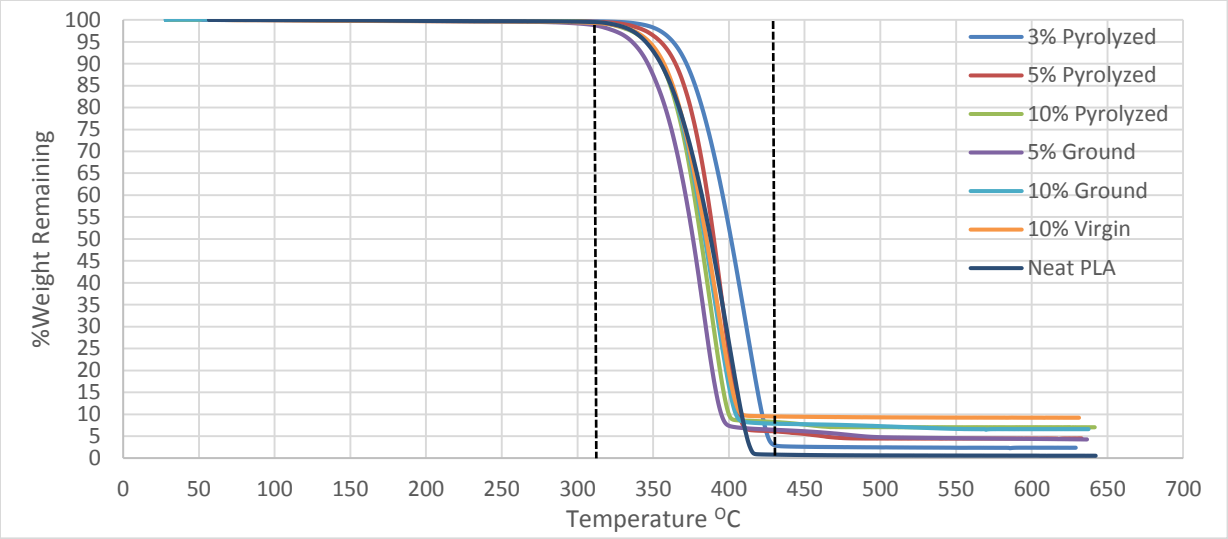

Figure 37: TGA graph that shows the fiber weight fraction for extruded filaments for the different reinforcement type with different reinforcement percentages

As shown, ground fibers had an average offset error almost equal to 30% while pyrolyzed fibers had almost half of that offset error. Virgin reinforced filament analysis showed that fiber weight fraction was 9.21% instead of 10%, which was the only reinforcement percentage that was used as a benchmark. The modified fiber weight fractions are summarized in table (7) and they have been used in updating the model that had been used in the previous work [89].

Table 7: Summarize the difference between the proposed reinforcement percentage and the actual percentage

Fibre Batch	%Fibre Weight Fraction	%Measured Weight Fraction	%Error
Pyrolyzed	3	2.96	1.3
	5	4.79	4.2
	10	8.30	17.0
Ground	5	4.25	15.0
	10	6.60	34.0
Virgin	10	9.21	7.9

When the pure PLA TGA graph is compared to other reinforced filament graphs, the degradation temperature range was almost identical which reveals that the reinforcement is not affecting the morphology of the PLA. Only one degradation step was observed for the neat PLA and other composites, and no significant change was captured with increasing fiber content.

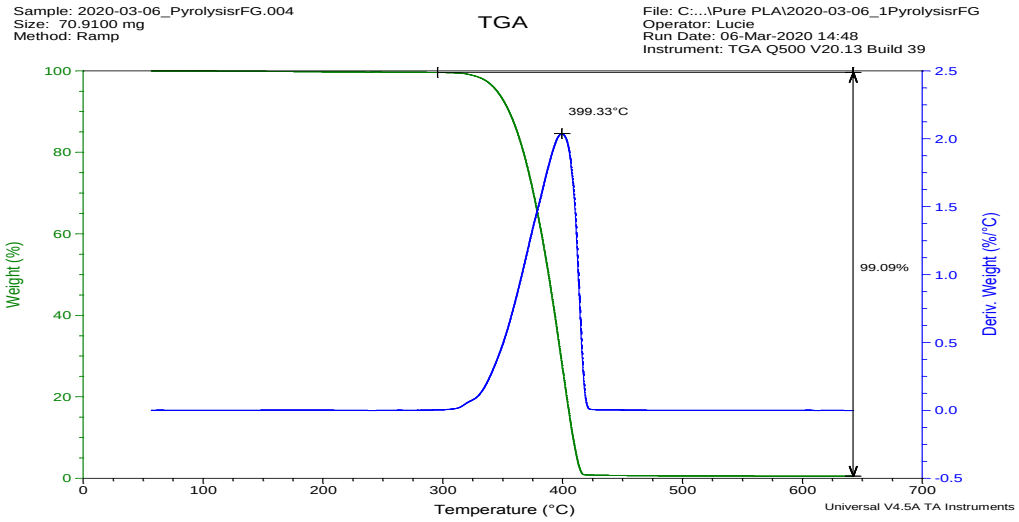

Figure 38: TGA graph for neat PLA sample

4.2.3. Single Fiber Tensile Test Results (σ_f, E_f)

The tensile properties of ground, pyrolyzed and virgin fibers with respect to the different gauge lengths are presented in Figure (39) along with error bars that show the maximum and minimum difference from the average values. Table (8) summarizes the mean values of single fiber tensile response, i.e. strength, stiffness and strain-to-failure. Unsurprisingly, a brittle failure mode was observed for the all tested fibers. Also, it had been noted that a reduction in the average failure strength is associated with higher fiber gauge lengths.

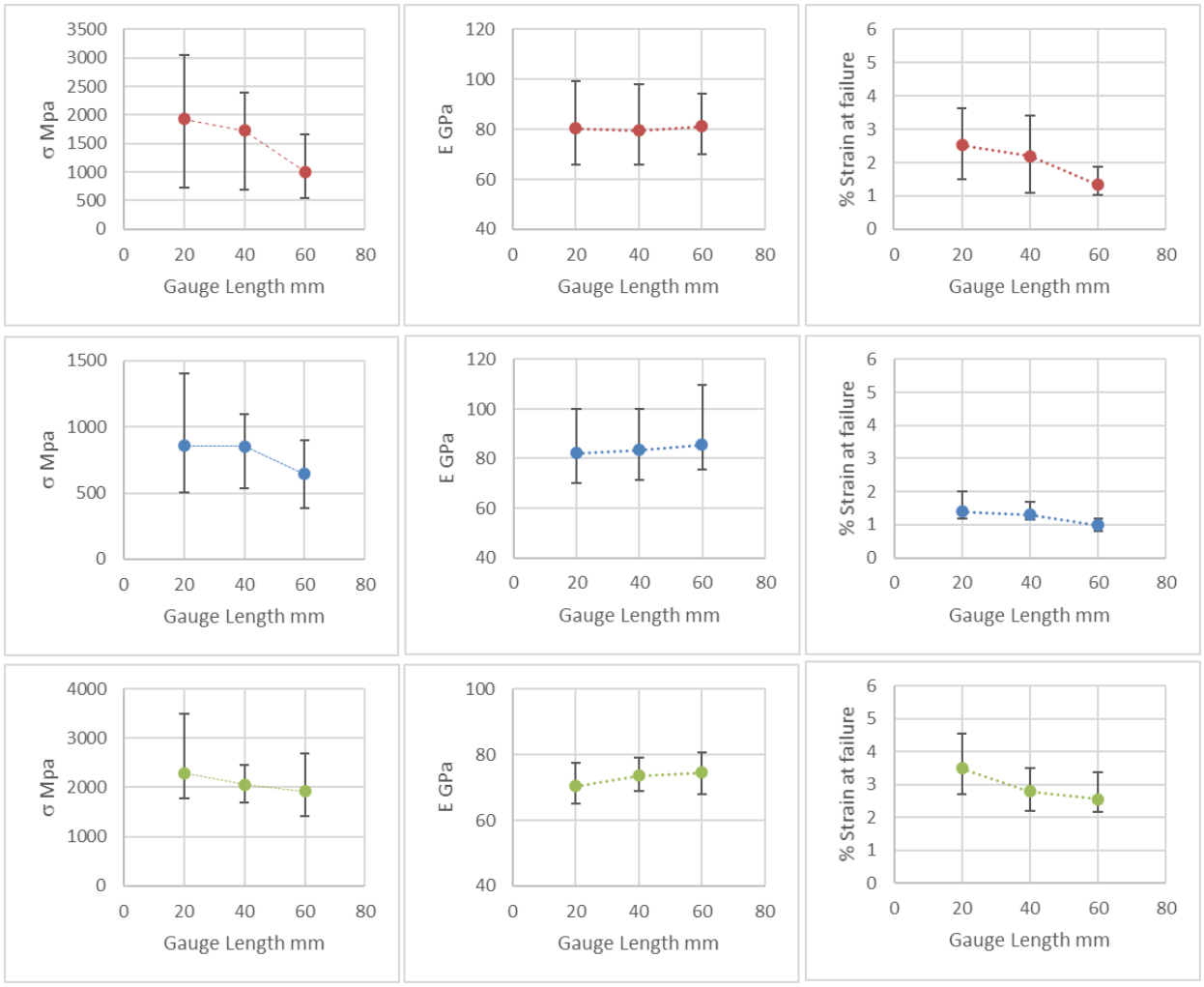

Figure 39: Tensile properties of ground fibers (First row), pyrolyzed fibers (second row), virgin fibers (third row)

An average 15% reduction in the average ultimate strength is further noted when increasing the gauge length from 20mm to 60mm for the ground fibers. Also, the same declining trend with a total drop of 30% in the average ultimate strength highlighted for the pyrolyzed fibers. Similarly, a reduction in mechanical properties of the virgin fibers is seen when the gauge length increases, which matches the same findings in the literature [88-89].

Table 8: Summary of the mean values & STD of the tensile properties of the different fibers tested

Fiber Type	Gauge Length mm	Mean Strength MPa	STD
Pyrolyzed	20	859	191
	40	853	173
	60	646	101
Ground	20	1932	759
	40	1730	558
	60	1011	345
Virgin	20	2295	322
	40	2063	211
	60	1923	272

Contrarily, longer fibers exhibited higher modulus compared to the shorter ones matching some findings in the literature [75-80]. The fiber stiffness at 60mm gauge length was higher than that of fibers with a gauge length of 20mm for both ground and pyrolyzed fibers. The same trend was observed for virgin fibers as well. The defect distribution on the fiber surfaces has a major influence on the mechanical performance of the fibers and the variation as well. In general, shorter fibers will likely feature lower quantities of surface flaws and microcrack formation compared to the longer ones. This results in more scattering of the data for the longer fibers.

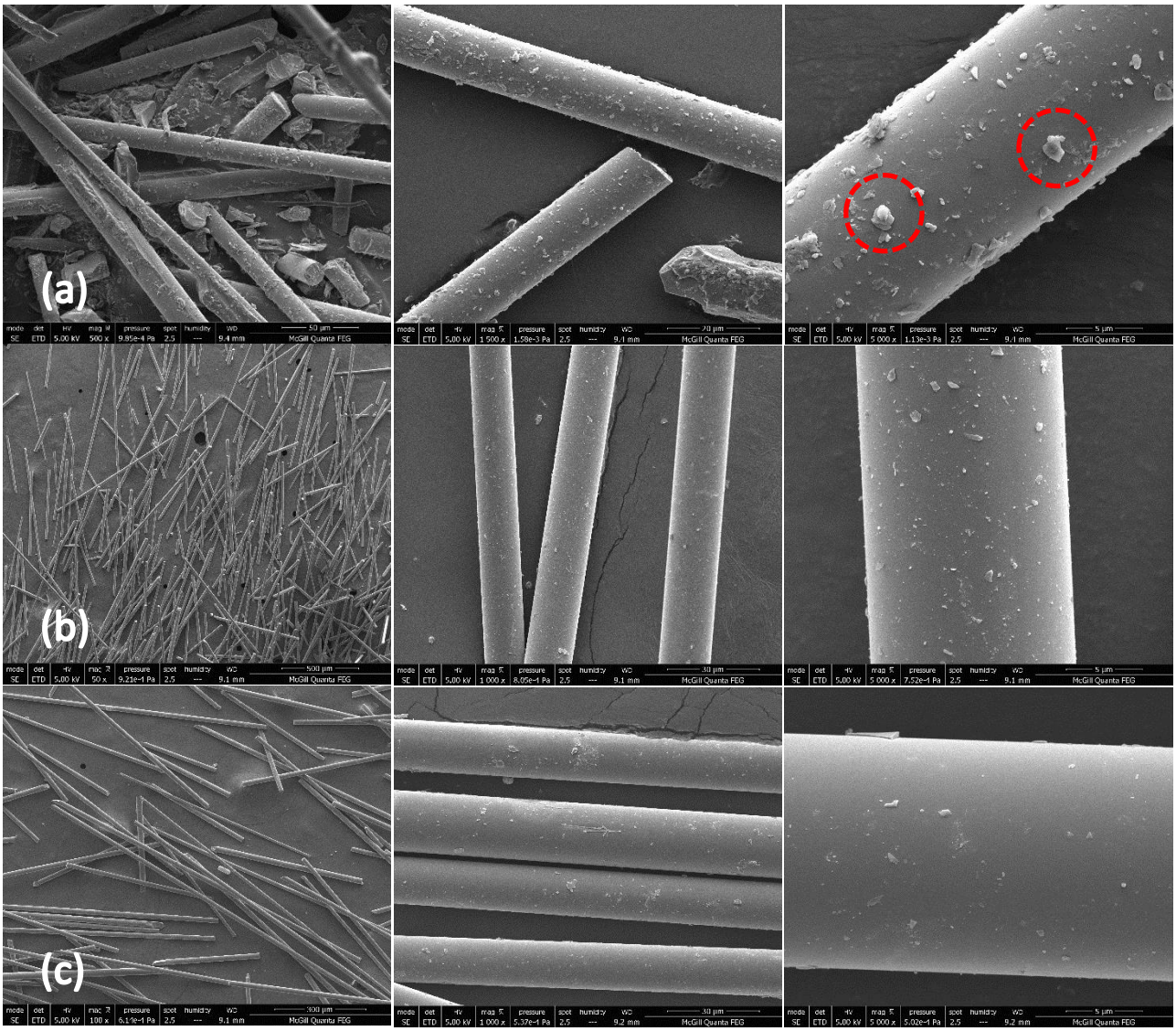

Figure 40: SEM Images for (a) ground fibres, (b) pyrolyzed fibres and (c) virgin fibres. Red circles indicate epoxy particles which contribute to surface roughness on ground fibres.

The average strength values for the ground fibers were 15.9%, 18% and 48% lower than the virgin fibers at 20mm, 40mm and 60mm gauge lengths, respectively. However, they showed higher strength values by 50%, 52% and 40% compared to the pyrolyzed fibers. Similarly, virgin fibers showed 60%, 61% and 65% higher values in tensile strength for gauge lengths of 20mm, 40mm and 60mm, respectively, in comparison to the pyrolyzed fibers. Strength improvement is predicted by removing the epoxy residues that can be considered as surface impurities.

However, this reduction can be attributed to the fact that E-glass properties are highly affected by the high processing temperatures frequently used in pyrolysis [93].

On the other hand, pyrolyzed fibers showed higher stiffness values compared to ground fibers with improvements equal to 9%, 11% and 17% for the 20, 40 and 60mm gauge lengths, respectively. However, the strain at failure was reduced by 47%, 56% and 43% for the different gauge lengths, indicating that pyrolyzed fibers are much more brittle in comparison to the ground fibers. According to [94], the molecular network will experience compaction during the thermal separation, i.e., the pyrolysis process, that will densify the fibers and result in improving the stiffness.

While these notable stiffness increases have been reported for pyrolyzed fibers, ground fibers showed slightly higher mean stiffness values compared to the virgin fibers. Generally, fibers exhibit significant strength variation corresponding to fiber diameter and length disparity. Strength variability is instigated due to the inherent flaw distribution along a fiber. In other words, there is no exact value for fiber strength. Thus, employment of a statistical distribution will help in defining a clear representation the fiber strength.

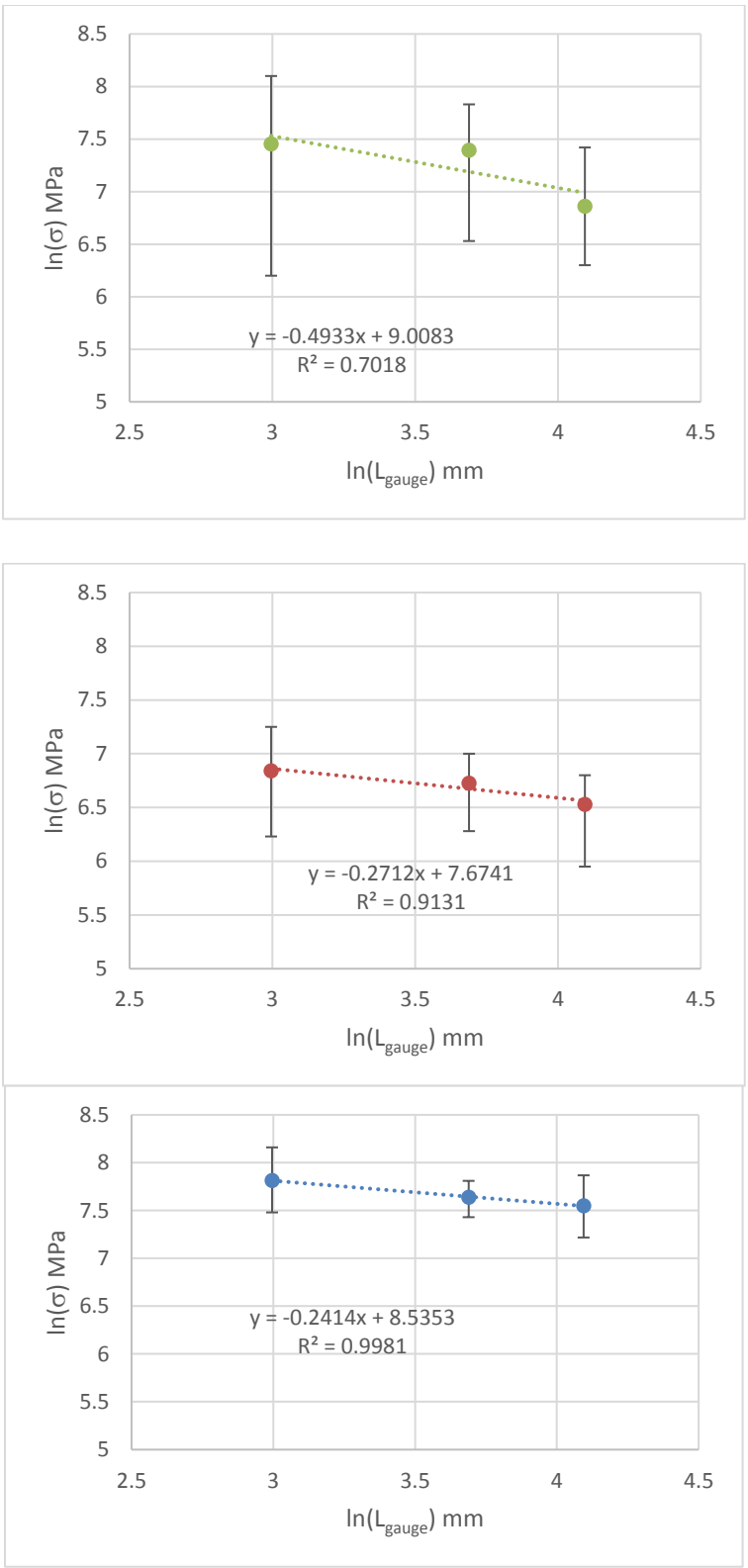

Figure 41: Strength variations at different gauge lengths for Ground (Top), Pyrolyzed (Middle), Virgin (Bottom).

The distribution of the failure stress of brittle fibers usually fits the standard Weibull model. Mainly, it is constructed on the idea of the weakest link failure, and it is well adopted in the literature [95]. In general, the Weibull function is used to represent the distribution of the strength values among the fiber batch. It is a clear method to show the variation of the values of strength within fiber batch. Both variations in strength at each specific gauge length as well as variations at different gauge lengths are shown in figure (41). The scale (σ_0) and shape (κ) parameters are used in the function as follows:

$$P(\sigma_f) = 1 - e^{[-(\frac{L}{L_0})(\frac{\sigma}{\sigma_o})^{\kappa}]} \quad (16)$$

where P(σ_f), is the cumulative failure probability of the fiber at the respective stress value σ_f and gauge length L. κ is the shape factor that indicates the variability of the data. A higher κ value indicates a narrower distribution while a lower κ corresponds to a wide distribution of fracture strength values. σ_0 is the reference Weibull strength at a specific reference gauge length L_o. To find the Weibull parameters, the strength data for each gage length is sorted in an ascending order and a probability function is used to identify the probability of fiber failure for the ith strength point, using the following equation:

$$P_i = \frac{i - 0.5}{N} \quad (17)$$

where N, is the number of data points, i represents the rank of the i_{th} number in the ascending ordered strength data point (i=1) corresponds to the smallest strength value while i = N corresponds to the highest value). By reorganising equation (16) and taking the natural logarithm of both sides, we obtain the subsequent expression:

$$\ln\left(-\ln\left(\frac{1}{(1-P(\sigma_f))}\right)\right) - ln\left(\frac{L}{L_o}\right) = \kappa\ln(\sigma) - \kappa\ln(\sigma_o) \quad (18)$$

For a constant length, L = L_o, Equation (18) is reduced to:

$$\ln\left(-\ln\left(\frac{1}{(1-P(\sigma_f))}\right)\right) = \kappa\ln(\sigma) - \kappa\ln(\sigma_o) \quad (18a)$$

By plotting X = βln(σ) VS Y = $\ln\left(-\ln\left(\frac{1}{(1-P(\sigma_f))}\right)\right)$ a straight line will be generated with a slope equal to the shape parameter (κ) and the scale parameter can be found from the y-intercept. Although there is some error between the fitted line compared to the experimental results, especially at the high and low strength extremes. The fitting parameters are summarized in table (9) for ground, pyrolyzed and virgin fibers.

Table 9: Scale and shape factors for the Weibull distributions for virgin, pyrolyzed and grounds fibers

Fiber Type	Gauge Length mm	Scale Factor	Shape Factor
Pyrolyzed	20	1072	4.278
	40	922.9	5.906
	60	750.1	6.569
Ground	20	2164	2.783
	40	1926	3.065
	60	1132	3.202
Virgin	20	2734	5.419
	40	2190	10.46
	60	2130	6.772

With highest values for both the scale and shape parameters, virgin fibers exhibited the highest properties and precision. Moreover, a larger shape parameter was found in pyrolyzed fibers in comparison to the ground fibers, corresponding to less scatter on the strength data points. The large discrepancy seen in ground fiber strength values is attributed to the presence of randomly distributed epoxy residues on fibers surfaces. This observation emphasizes the role of the resin residues by generating stress concentration zones that will reduce the fiber strength. Also, the grinding process can cause surface microcracks that will be responsible for lowering the fiber strength. Correspondingly, the pyrolyzed fibers displayed lower strength than the reported values in the literature [96].

4.2.4. Interfacial Strength Test Results τ_{IFSS}

It is not easy to conduct a successful pull-out test, so unsuccessful tests that feature two failure modes should be eliminated. These are when there is a fiber break before the failure at the interface or when a test fails at the fiber ends/grips. Based on that, the samples were inspected after performing the tests to inspect for any kind of irregularities. Determination of the interfacial shear strength is governed by finding the interface failure force $F_{failure}$ with the respect to at the specific embedded length of fiber attached to the matrix $L_{embedded}$ and fiber diameter d_i, using to the following equation:

$$\tau_{IFSS} = \frac{F_{failure}}{\pi d_i L_{embedded}} \tag{19}$$

where $L_{embedded}$ was estimated by determining the thickness of the interface, while the maximum force reported in the force vs. displacement curve was assigned to be $F_{failure}$. A total

of 20 pull-out tests were performed for each fiber batch, i.e., ground, pyrolyzed and virgin and the τ_{IFSS} with error bars are presented in figure (42).

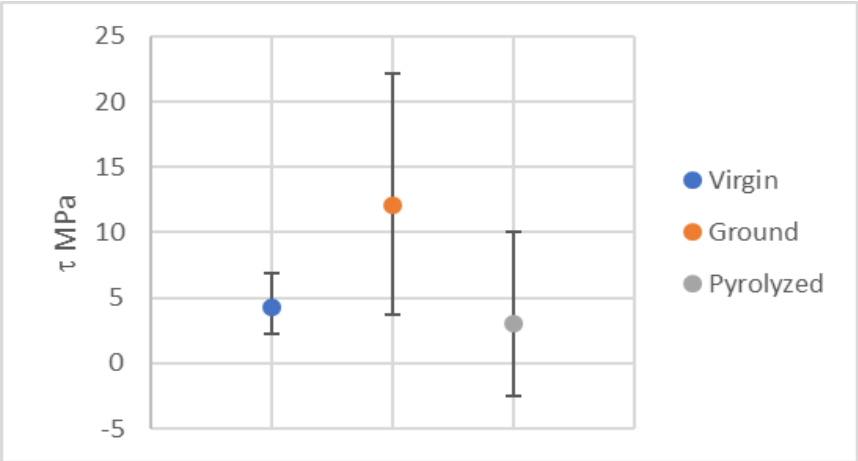

Figure 42: Mean τ_{IFSS} values for the different fiber batches

Table 10: Summary of the mean values of τ_{IFSS} and the standard deviation

Fiber Batch	τ_{IFFS} MPa	STD
Virgin	4.2	1.5
Ground	12.0	4.7
Pyrolyzed	8.2	3.5

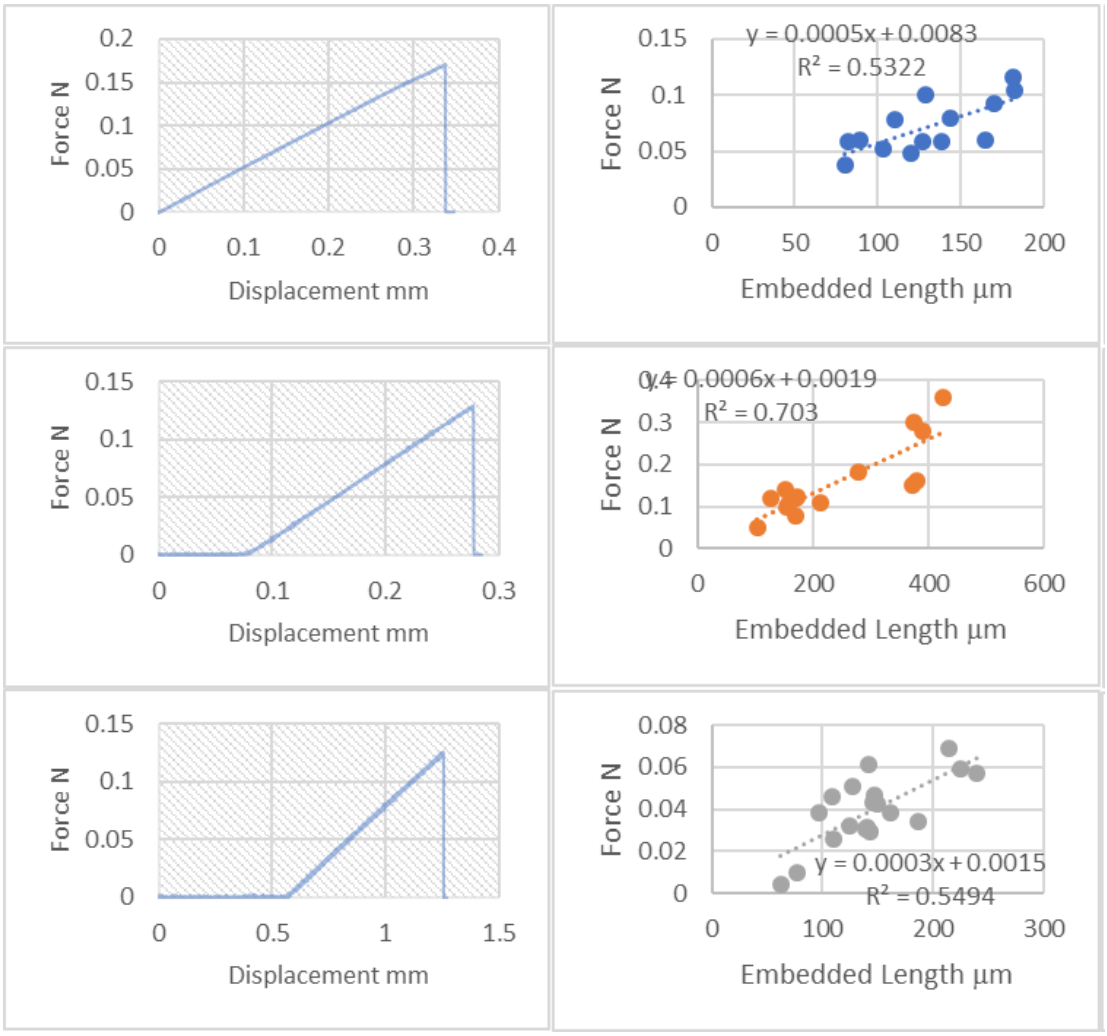

Figure 43: Representative force-displacement curves vs. embedded length plots of single fiber pull out test for PLA and: (first row) pyrolyzed fibers; (second row) ground fibers; (third row) virgin fibers

The force vs. displacement curves are used to determine the shear strength at the interface between the fiber and the matrix. The mean values of the interfacial shear strength and the associated standard deviation for the virgin, ground, and pyrolyzed fibers are tabulated in Table 10. The ground fibers exhibited the highest IFSS corresponding to a stronger bond at the interface. Virgin fibers had the lowest IFSS equal to 4.2 MPa which is a 48.8% and 65.1%

lower IFSS compared to the pyrolyzed and ground fibers, respectively. Although no definitive benchmark exists for minimum IFSS, the higher this value is, the better.

The higher IFSS values for the ground fibers are attributed to the presence of epoxy impurities on the fiber surfaces resulting in higher surface roughness. Moreover, higher mechanical interactions and interlocking mechanisms will more likely be to be found at the fiber/PLA interface [88]. It also can be noted from table (10) that ground fibers have the highest standard deviation, which is also attributed to the existence of random epoxy residues on the fiber surfaces.

4.3. ASTM D638-a Test Results

Typical stress vs. strain curves for the tested coupons are presented in figure (44). Clearly, the effect of increasing the % of reinforcement fibres improved the tensile stiffness of the material compared to the neat PLA. It can be seen that, all the fibre-reinforced batches failed in a brittle manner at lower strain than pure PLA with maximum failure strains equal to 2% reported for all tested samples. The ultimate strength was recorded for the neat PLA and the reinforced coupons.

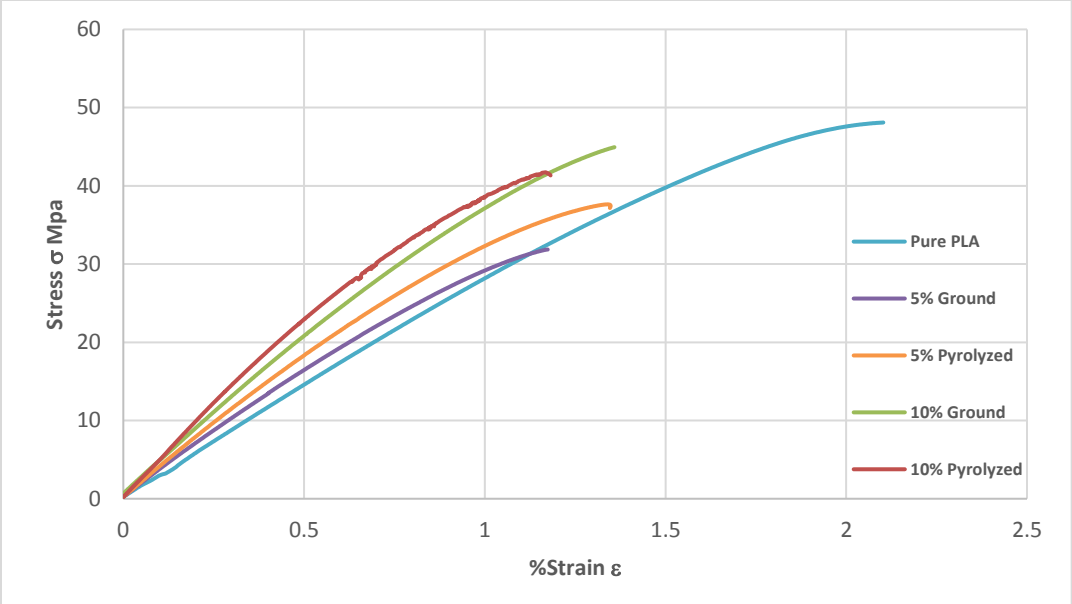

Figure 44: stress vs strain curves for the tested specimens

4.3.1. Specific Stiffness

Figure (45) illustrates the normalized specific properties of the 3D printed coupons as a function of weight variations of the tested samples. For the specific tensile stiffness, all the different fibre batches showed a higher mean specific tensile stiffness, which increased at higher fibre content. Note that PLA reinforced with virgin fibres showed the lowest mean specific stiffness compared to ground and pyrolyzed fibres. Pyrolyzed reinforced coupons exhibited higher stiffness values compared to ground fibres with improvements equal to 19.2% and 16.5% for the 5 and 10% fibre weight fractions, respectively. The variation of the fibre length, resin powder, as well as the inconsistency of the fibres surface roughness are the main contributors to the standard deviation (STD) values which are presented as the error bars in figures (44,45,46). Young's modulus showed a significant reliance on fibre content and fibre aspect ratio compared to the fibre orientation and fibre/matrix adhesion, which had been discussed extensively in the literature [100-102]. It is important to note that the increase in the

fibre content is directly proportional to the stiffening of the final composite, and the introduction of some impurities that increase the constraints within the geometry will result also result in a more stiff material, as discussed in previous studies [88].

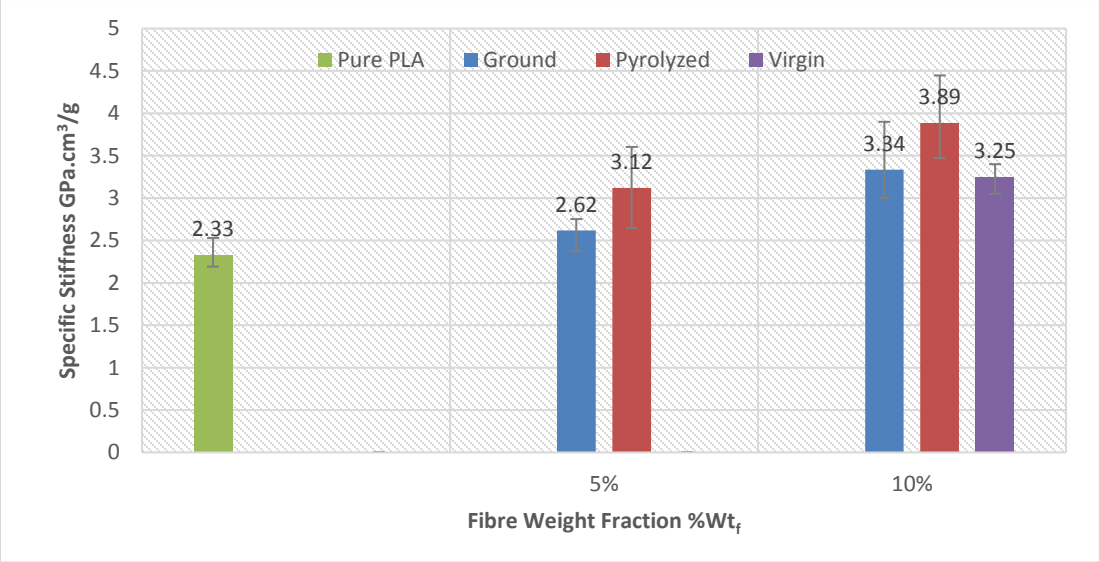

Figure 45: Tensile specific stiffness of glass fibre reinforced specimens with different fibre content,

4.3.2. Strain at Failure

The results for strain at failure are shown in figure (46). All reinforced coupons had lower stain at failure values compared to the neat PLA coupons. In fact, pyrolyzed coupons showed the lowest failure strain compared to virgin and ground fibres. Their reduced ductility (caused by the pyrolysis process) could be the cause of the lower failure strain in the final composite [88]. During the thermal treatment of the fibres during pyrolysis, the molecular network will experience a compaction behavior which will densify them resulting in more stiff but brittle fibres [94].

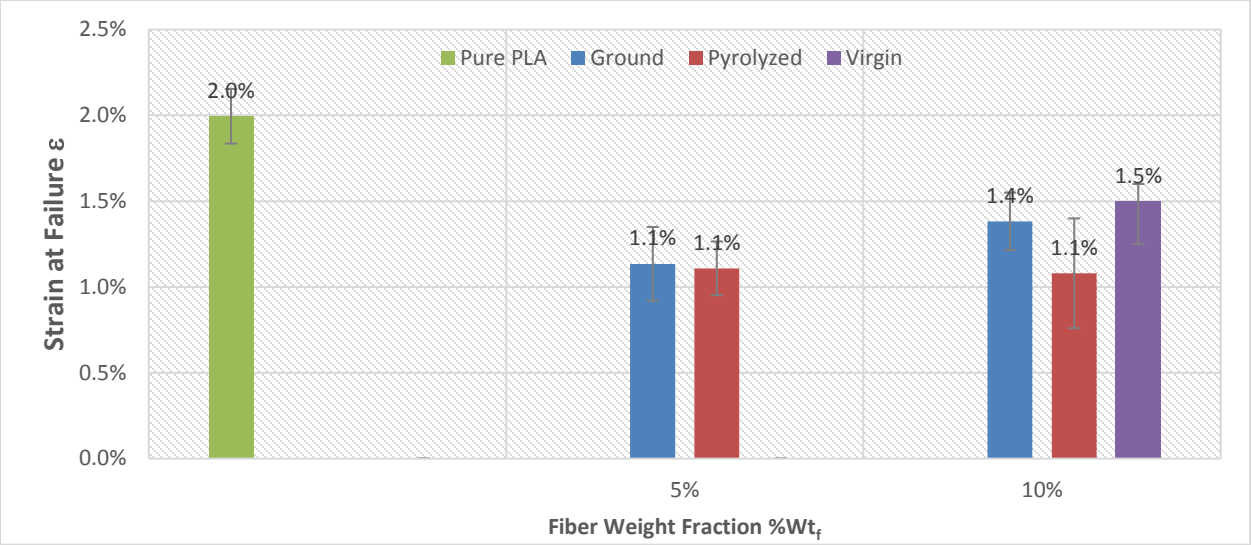

Figure 46: Tensile strain at failure of glass fibre reinforced specimens with different fibre content.

4.3.3. Specific Strength

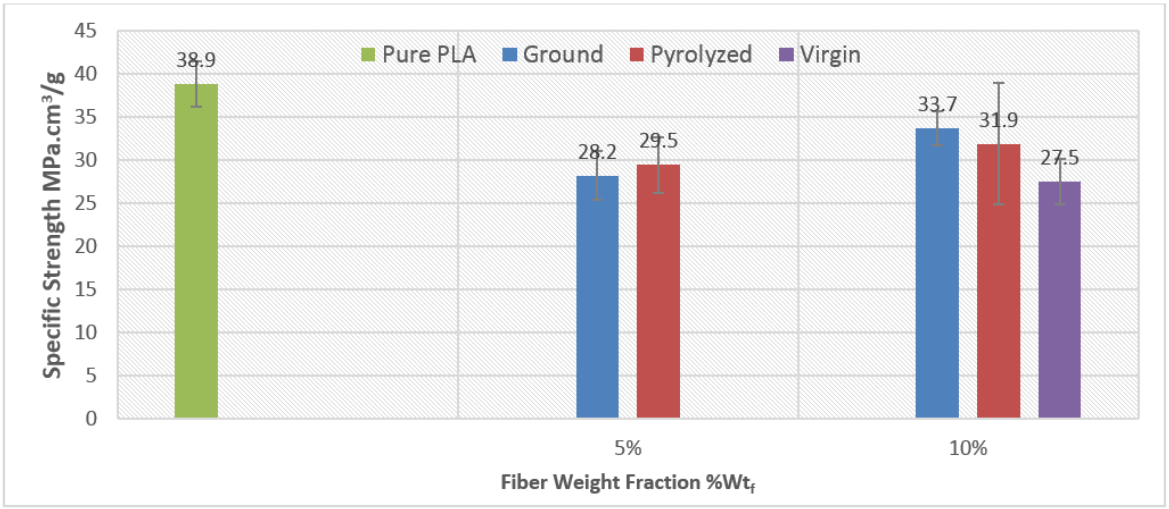

Figure 47: Tensile specific strength of glass fibre reinforced specimens with different fibre content.

Maximum tensile strength was measured in pure PLA coupons at 38.9 MPa.cm^3/g. A good uniformity in the results is indicated by the small error bars shown in figure (47). For the fibre-

reinforced results, there is an inversely proportional relation between the fibre content and the reported strength values. In other words, the higher fibre weight fraction used, the lower the measured strength in the composite. Reduction of strength could be attributed to many factors including fibre agglomeration and the increase of fibre-fibre interaction due to the improper fibre wetting. Also, the increase in porosity in the geometry [103] could be a factor, even though it is unlikely to be controlled. However, limiting lower fibre-fibre interaction and attaining better fibre wetting can be achieved by controlling the polymer viscosity [104].

4.4. Micromechanical Models – Comparison Between the Predicted and the Actual Composite Tensile Properties

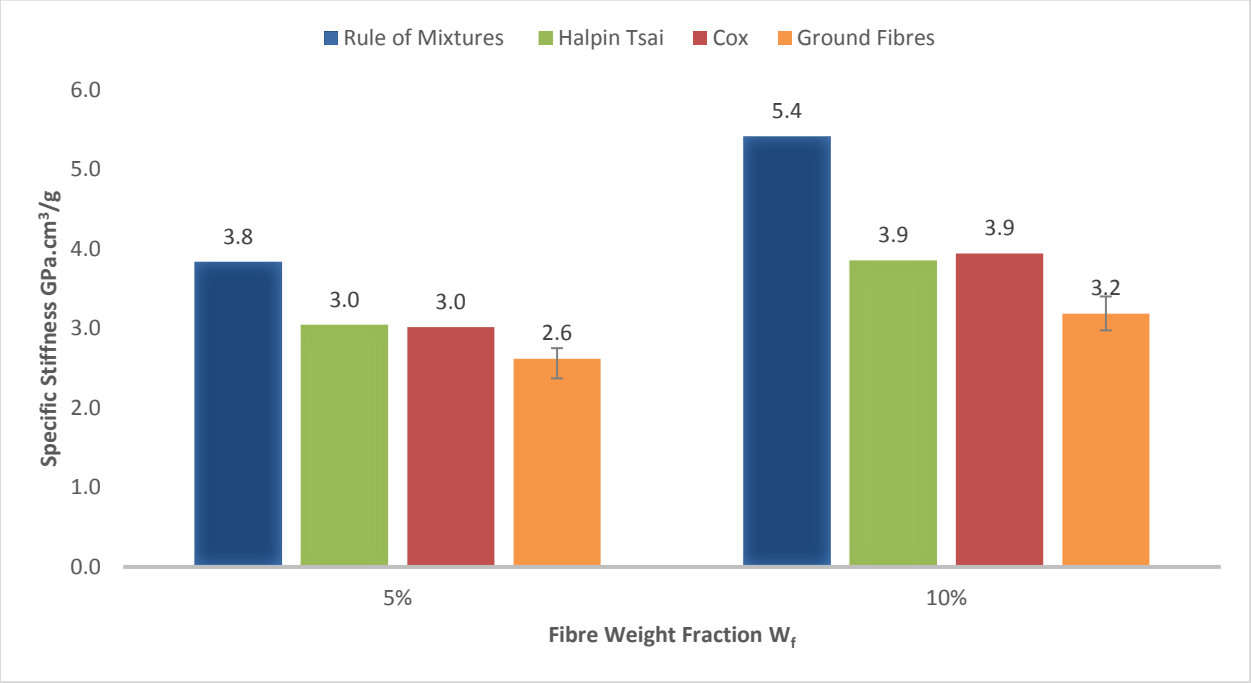

Figure 48: Normalized tensile specific stiffness results for the ground coupons: RoM (blue), Halpin-Tsai (Green), Cox (Red) and experimental results (Orange).

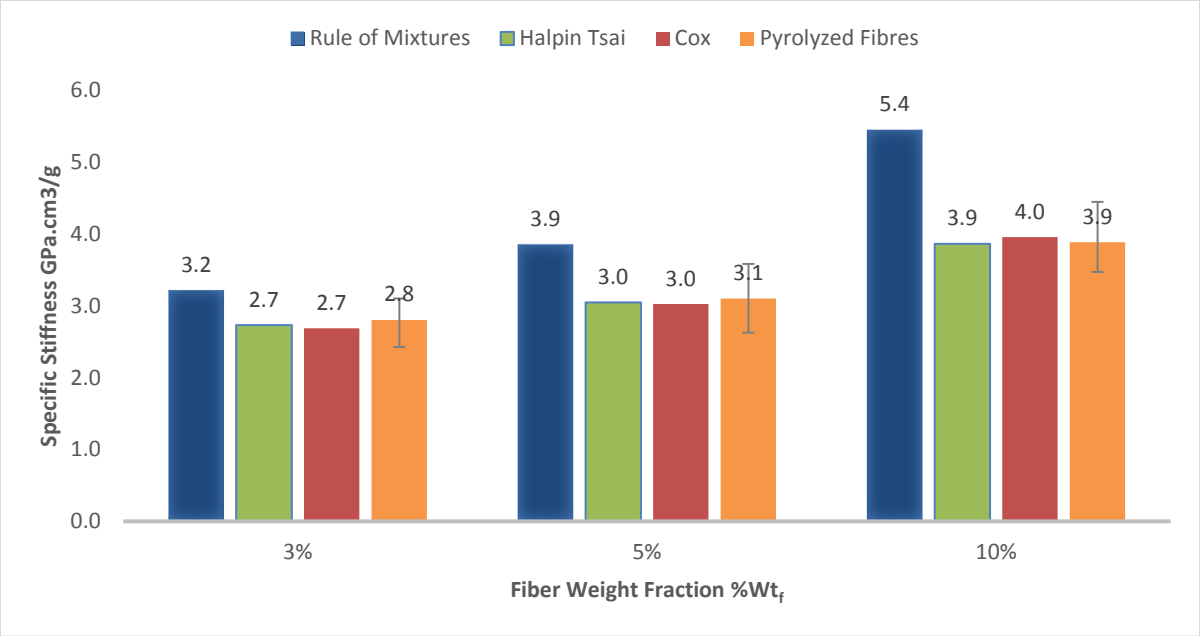

Figure 49: Normalized tensile specific stiffness results for the pyrolyzed coupons: RoM (blue), Halpin-Tsai (green), Cox (red) and experimental results (orange).

Ground recycled fibres, pyrolyzed and virgin fibres were then used to reinforce PLA (Polylactic polymer) without any additional pre-treatment of the fibre surfaces. Levels of 5% and 10% reinforcement were used to study the effect of the fibre weight fraction on the mechanical properties of the composite. Several models were established in order to verify that models are a useful tool to predict the tensile properties of these recycled filaments. As mentioned earlier, a simple micromechanical model can be a useful tool in order to minimize the experimental validation of future work. Although the models used are simple, they have been used extensively in the literature for several types of reinforcements. Several initial parameters were discussed earlier to eliminate any error introduced by having wrong initial

values. In this work, Rule of Mixtures, Halpin-Tsai, Cox models are used to predict the strength and the stiffness of the 3D printed coupons with different reinforcement type and content. The results are normalized by weight due to the density variation of the 3D printed samples in Figures (48) and (49).

4.4.1. Specific Stiffness

Figure (48) shows a comparison between the experimental stiffness for PLA/Ground fibres at different fibre contents and the fitted (Modified Rule of Mixtures, Halpin-Tsai, and Cox) models. All models predicted higher strength values compared to the experimental results. The Rule of Mixtures fit showed the highest prediction compared with the other models with 1.2 to 2.2GPa difference higher than the actual experimental values. One of the main reasons for this high error is that the RoM is independent of the reinforcement geometry and their distribution within the matrix. Moreover, it neglects the interaction between the constituents due to the difference of the Poisson's ratios.

The Cox and Halpin-Tsai models showed a better prediction with maximum difference reported equal to 0.7 GPa. Both of the models assume a perfect bonding at the interface. Halpin-Tsai considers the effect of the reinforcement aspect ratio and the volume fraction of the reinforcement in a simple straightforward way [76]. The prediction showed an offset difference equal to 0.4 and 0.7 GPa for 5% and 10% fibre weight fraction, respectively. Several

studies highlighted the important effect of the fibre aspect ratio on the stiffness of the composite [104]. The Cox model assumes a perfect elastic behavior of both the fibre and the matrix. It was developed based on the shear lag theory which suggests that the shear stress at the fibre/matrix interface region will be responsible for transferring the load to the fibres [80]. It adds an effective load transfer factor to the RoM theory, which includes fibre radius, shear modulus of the matrix, area of the fibres and the centre-to-centre distance of neighboring fibres. This model showed very similar results to Halpin-Tsai model and that could be attributed to the fact that both models are considering the effect of the fibre aspect ratio and the packaging factor on the stiffness. However, there is still an offset error introduced in these predictions and that could be attributed to the presence of the epoxy particles that cause a disparity of the surface roughness of the ground fibres; typical epoxy particles can be seen in figure (40a). Subsequently, the comparison between the experimental composite stiffness for PLA/Pyrolyzed fibres at different fibre contents and the fitting models are presented in figure (49). Similar to the ground fibre coupons, the RoM fit showed the highest predicted stiffness results compared to the other models. A level of 0.4 and 1.5GPa difference was reported for 5 and 10%Wt_f, respectively. The Halpin-Tsai model showed good predictions with an error of less than 2.1%, 3.5% and 2.8% for 3%, 5% and 10%Wt_f, respectively. Cox showed promising good predictions with errors of less than 3.6%, 6.5% and 2.8%. It is interesting to highlight that

models became more accurate without resin particles in the recyclate. This is expected, since the models that were used to predict the ground fibre composite stiffnesses did not consider the effect of the presence of the epoxy residues.

4.4.2. Specific Strength

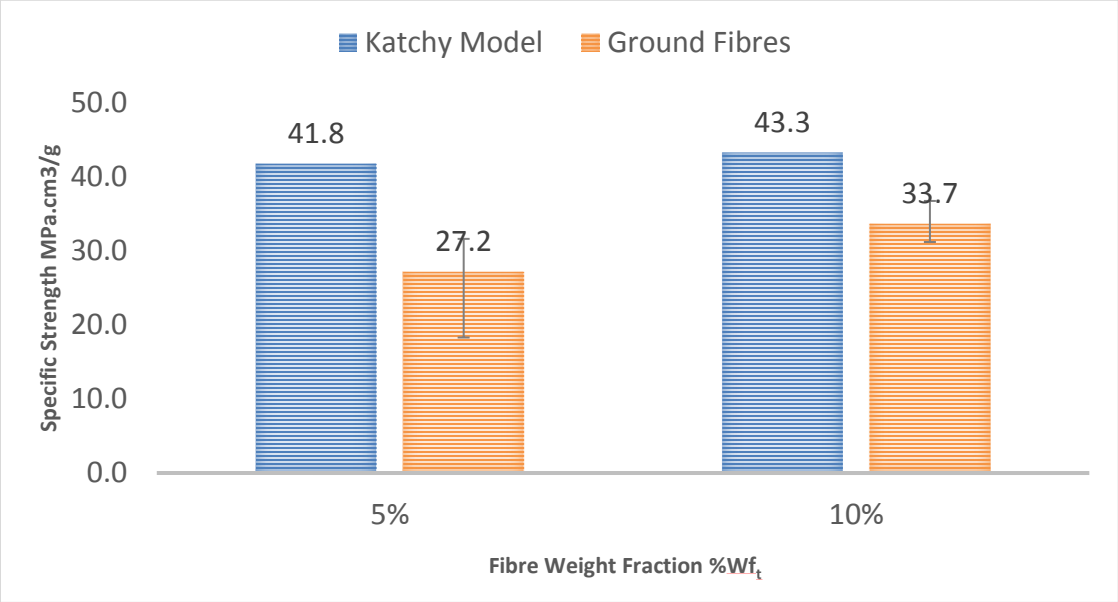

Figure 50: Normalized tensile specific strength results for the ground coupons: Katchy (blue) and experimental results (orange).

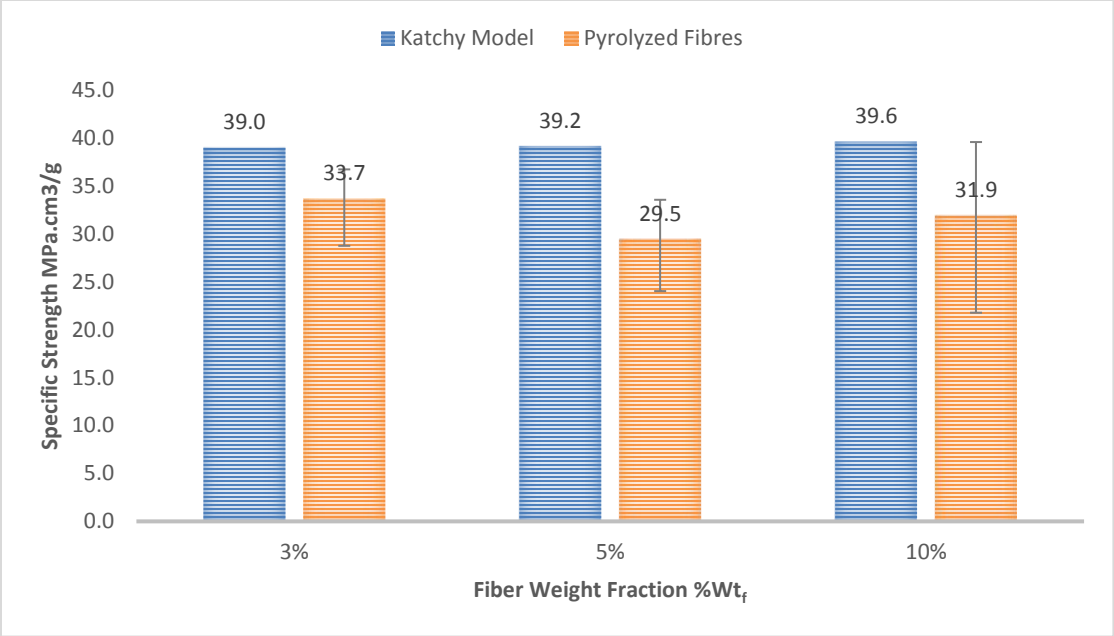

Figure 51: Normalized tensile specific strength results for the pyrolyzed coupons: Katchy (blue) and experimental results (orange).

Short fibre composite strength is similar to stiffness in that they are both functions of the fibre aspect ratio. However, unlike stiffness, strength depends heavily on the interfacial adhesion of the fibres. The better the adhesion, the higher the stress that the composite can reach before it fails [104]. In this work, the experimental results of the specific strength are compared to a modified model proposed by Katchy [77], which introduces the interfacial strength in the prediction of the composite ultimate strength. Figures (50,51) show the specific experimental strength results and predictions as a function of $\%Wt_f$. Slightly higher values were predicted compared to the actual experimental results. Pyrolyzed fibres showed a better prediction with errors equal to 15.7, 32.9 and 24.1% for 3, 5 and 10 $\%Wt_f$. On the other hand, 53.7% and 28.5% differences were reported in results for 5 and 10 $\%Wt_f$ of ground fibres. This comparison is an indication of the negative effect of the epoxy residues on the prediction

accuracy. It is also important to highlight that the dispersion of the fibres within the matrix will affect the effectiveness of the fibre adhesion. The more dispersed fibres will limit the fibre/fibre interactions and that will limit the chance of having dry unbonded locations as can be seen in figure (52).

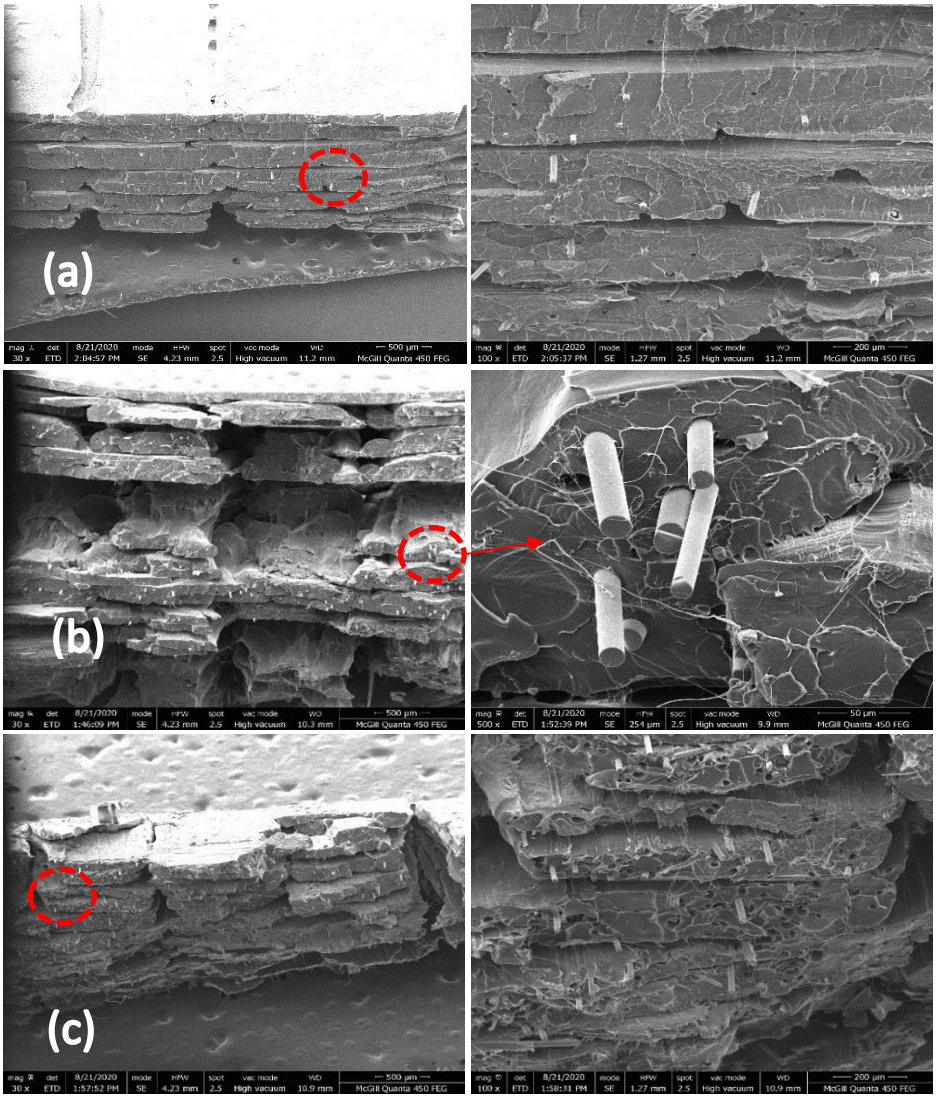

Figure 52: SEM Images for the fracture surface of the pyrolyzed reinforced tested coupons (a) 3%, (b) 5% and (c) 10%Wt_f. Red circles highlight the fibres agglomeration at the higher reinforcement fraction.

The variation of the aspect ratio will influence the composite strength. For fibres with lower AR, a lower applied load is required to pull fibres out of the matrix $\overline{\sigma}_f = \tau_i \frac{l_f}{d_f}$. By assuming that the failure will happen once the applied stress σ_{app} reaches the maximum stress that can be applied before one of the fibres will fail at the interface, then $\sigma_{app} \times \frac{d_f}{l_f} = \tau_i$. Since τ_i is a material property, we can use the average value as a fixed value for all fibres. As a result, the lower the AR will be, the higher the reciprocal AR^{-1}, which will lower the range of the load that can be applied before reaching interface failure. Using the lowest AR (3.77), which was reported in an earlier section, the lowest applied stress needed to imitate the failure at the interface will be equal to 30.9 MPa.

5. Summary and Conclusion

5.1. Summary

In summary, this work investigated the effect on strength and stiffness of the incorporation of recycled fibreglass, reclaimed from end-of-life wind turbine blades, into PLA that was used in Fused Deposition Modeling (FDM). A full comparison, in terms of strength and stiffness on the different tested fibre categories was presented and discussed to define the most feasible candidate to reinforce PLA filament. In total, three different fibre categories (i.e. virgin, ground and pyrolyzed fibres) were examined and compared. The effect of increasing the % of reinforcement fibres improved the tensile stiffness of the material compared to the neat PLA. Ground recycled fibres (GRF) showed higher ultimate tensile strength compared to pyrolyzed and virgin fibres. However, higher stiffness values were obtained for Pyrolyzed fibres compared to ground and virgin fibres. In addition, this study also compared the mechanical performance of Polylactic Acid/recycled Glass Fibre (PLA/rGF) aligned discontinuous composites assessed experimentally to simple elastic micromechanical prediction models (Rule of Mixtures, Halpin-Tsai and Cox models). A significant deviation from the theoretical model was observed on ground fibres/PLA coupon response compared to pyrolyzed fibres, which can be the result of the presence of epoxy residues within the recyclate. These simple models can be useful prediction tools for the stiffness compared to the strength since the degree-of-adhesion is not a significant factor for the Young's modulus prediction. Thus, the composite modulus will be essentially independent of the adhesion compared to the strength, which is significantly affected by the degree-of-adhesion. Finally, simple models can be useful prediction tool for the stiffness compared to the strength since the degree-of-adhesion is not a significant factor for the Young's modulus prediction. Thus, the composite modulus will be essentially independent

of the adhesion compared to the strength which is significantly affected by the degree of the adhesion.

5.2. Conclusion

Our findings have shown that the use of recycled fibres can significantly increase the specific modulus of the 3D printed specimens reinforced with recycled glass fibres components. It was found that using recycled fibreglass to reinforce PLA filament has promising outcomes in terms of stiffness improvement. In fact, the mean specific stiffness has improved by 69.6%, 43.1% and 39.5% for 10% reinforced tested coupons for pyrolyzed, ground and virgin fibres, respectively. By contrast, the addition of the fibres had a detrimental effect on the samples' ductility and their ultimate strength. This led to a significant average drop of 25.4% and 20.3% in the ultimate strength that was measured for 5 and 10 $\%Wt_f$. Comparison between experimental results and the predictions from theory for the tensile properties of composites reinforced with different fibre types have been also presented. Cox and Halpin-Tsai models gave a good agreement with the experimental tensile stiffness results compared to the simple Rule of Mixtures model. They both gave a good agreement with the experimental values with variation of less than 10%. Subsequently, the Katchy proposed strength model showed a reasonable prediction for the composite strength with a maximum disparity equal to 35%, which can be directly related to the variation of fibre aspect ratios. Finally, both recycled fibres, i.e., ground and pyrolyzed fibres, exhibited higher strength and stiffness values compared to virgin fibres, which indicates that reusing recycled fibreglass from an end-of-life wind turbine blade is not only an environmentally encouraging solution, but also a competitor to other FDM 3D printing materials in the 3D printing market.

5.3. Future Work

Incorporating recycled fibreglass from WTB with PLA can be great solution to both the 3D printing market as well as the huge amount of WTB waste available. However, More work is required to fully establish a process that can be upscaled and reach the commercial levels. While the proposed recycling method in this work discussed the potential of reusing fibreglass reclaimed form end-of-life wind turbine blades, this scheme could be also extended to other fibreglass waste sources.

Moreover, utilizing more advanced sorting and grading of the fibres could limit the significant variation in the strength and the stiffness and improve the precision in the proposed models. Thus, more work should be carried out to study the effect of sorting. Finally, higher fibres aspect ratios could be used with the goal of achieving higher mechanical properties for the generated filament.

References

1. Tchana Toffe, G., Oluwarotimi Ismail, S., Montalvão, D., Knight, J., & Ren, G. (2019). A Scale-up of Energy-Cycle Analysis on Processing Non-Woven Flax/PLA Tape and Triaxial Glass Fibre Fabric for Composites. Journal of Manufacturing and Materials Processing, 3(4), 92. https://doi.org/10.3390/jmmp3040092
2. Baas, L. W., & Boons, F. A. (2004). An industrial ecology project in practice: exploring the boundaries of decision-making levels in regional industrial systems. Journal of Cleaner Production, 12(8–10), 1073–1085. https://doi.org/10.1016/j.jclepro.2004.02.005
3. Nijssen, R. P. L., & Brøndsted, P. (2013). Fatigue as a design driver for composite wind turbine blades. Advances in Wind Turbine Blade Design and Materials, 175–209. https://doi.org/10.1533/9780857097286.2.175
4. Beauson, J., & Brøndsted, P. (2016). Wind Turbine Blades: An End of Life Perspective. MARE-WINT, 421–432. https://doi.org/10.1007/978-3-319-39095-6_23
5. Yang, L., Sáez, E. R., Nagel, U., & Thomason, J. L. (2015). Can thermally degraded glass fibre be regenerated for closed-loop recycling of thermosetting composites? Composites Part A: Applied Science and Manufacturing, 72, 167–174. https://doi.org/10.1016/j.compositesa.2015.01.030
6. Karuppannan Gopalraj, S., & Kärki, T. (2020). A review on the recycling of waste carbon fibre/glass fibre-reinforced composites: fibre recovery, properties and life-cycle analysis. SN Applied Sciences, 2(3), 433. https://doi.org/10.1007/s42452-020-2195-4
7. Vo Dong, P. A., Azzaro-Pantel, C., & Cadene, A.-L. (2018). Economic and environmental assessment of recovery and disposal pathways for CFRP waste management. Resources, Conservation and Recycling, 133, 63–75. https://doi.org/10.1016/j.resconrec.2018.01.024
8. Oliveux, G., Dandy, L. O., & Leeke, G. A. (2015). Current status of recycling of fibre reinforced polymers: Review of technologies, reuse and resulting properties. Progress in Materials Science, 72, 61–99. https://doi.org/10.1016/j.pmatsci.2015.01.004
9. Kalkanis, K., Psomopoulos, C. S., Kaminaris, S., Ioannidis, G., & Pachos, P. (2019). Wind turbine blade composite materials - End of life treatment methods. Energy Procedia, 157, 1136–1143. https://doi.org/10.1016/j.egypro.2018.11.281
10. C Mattsson et al. (2020). IOP Conf. Ser.: Mater. Sci. Eng. 942 012013
11. Liu, P., & Barlow, C. Y. (2017). Wind turbine blade waste in 2050. Waste Management, 62, 229–240. https://doi.org/10.1016/j.wasman.2017.02.007
12. Larsen, K. (2009). Recycling wind turbine blades. Renewable Energy Focus, 9(7), 70–73. https://doi.org/10.1016/s1755-0084(09)70045-6
13. Job, S. (2013). Recycling glass fibre reinforced composites – history and progress. Reinforced Plastics, 57(5), 19–23. https://doi.org/10.1016/s0034-3617(13)70151-6
14. Gu, D. D., Meiners, W., Wissenbach, K., & Poprawe, R. (2012). Laser additive manufacturing of metallic components: materials, processes and mechanisms. International Materials Reviews, 57(3), 133–164. https://doi.org/10.1179/1743280411y.0000000014

15. Blok, L. G., Longana, M. L., Yu, H., & Woods, B. K. S. (2018). An investigation into 3D printing of fibre reinforced thermoplastic composites. Additive Manufacturing, 22, 176–186. https://doi.org/10.1016/j.addma.2018.04.039
16. Heidari-Rarani, M., Rafiee-Afarani, M., & Zahedi, A. M. (2019). Mechanical characterization of FDM 3D printing of continuous carbon fiber reinforced PLA composites. Composites Part B: Engineering, 175, 107147. https://doi.org/10.1016/j.compositesb.2019.107147
17. Egbo, M. K. (2020). A fundamental review on composite materials and some of their applications in biomedical engineering. Journal of King Saud University - Engineering Sciences. https://doi.org/10.1016/j.jksues.2020.07.007
18. Callister, W. D., & Rethwisch, D. G. (2018). Materials Science and Engineering. Wiley.
19. Altenbach, H., Altenbach, J., & Kissing, W. (2018). Mechanics of Composite Structural Elements (2nd ed. 2018 ed.). Springer.
20. Chung, D. D. L. (2013). Composite Materials. Springer Publishing.
21. Das, Sujit, Warren, Josh, West, Devin, and Schexnayder, Susan M. Global Carbon Fiber Composites Supply Chain Competitiveness Analysis. United States: 2016. Web. https://doi.org/10.2172/1333049
22. Glass Fiber Market Report: Trends, Forecast and Competitive Analysis. (2020, August). Lucintel. https://www.lucintel.com/glass-fiber-market.aspx
23. Duflou, J. R., Deng, Y., Van Acker, K., & Dewulf, W. (2012). Do fiber-reinforced polymer composites provide environmentally benign alternatives? A life-cycle-assessment-based study. MRS Bulletin, 37(4), 374–382. https://doi.org/10.1557/mrs.2012.33
24. Staff, C. A. H., Chapman and Hall Staff, Lubin, G., & Peters, S. T. (1998). Handbook of Composites. Springer Publishing.
25. Global Wind Energy Council. (2018). GLOBAL WIND REPORT 2014. https://gwec.net/publications/global-wind-report-2/global-wind-report-2014-annual-market-update/
26. WindEurope asbl/vzw. (2016). Wind energy scenarios for 2020. WindEurope. https://windeurope.org/about-wind/reports/wind-energy-scenarios-2020/
27. Renewable Energy Cost Analysis - Wind Power. (2012, June). IRENA. https://www.irena.org/publications/2012/Jun/Renewable-Energy-Cost-Analysis---Wind-Power
28. Gielen, D., Boshell, F., Saygin, D., Bazilian, M. D., Wagner, N., & Gorini, R. (2019). The role of renewable energy in the global energy transformation. Energy Strategy Reviews, 24, 38–50. https://doi.org/10.1016/j.esr.2019.01.006
29. Global Energy Transformation: A Roadmap to 2050 (2018 edition). (2018, April). IRENA. https://www.irena.org/publications/2018/Apr/Global-Energy-Transition-A-Roadmap-to-2050
30. Omer, A. M. (2009). Energy use and environmental impacts: A general review. Journal of Renewable and Sustainable Energy, 1(5), 053101. https://doi.org/10.1063/1.3220701
31. Ferronato, N., & Torretta, V. (2019). Waste Mismanagement in Developing Countries: A Review of Global Issues. International Journal of Environmental Research and Public Health, 16(6), 1060. https://doi.org/10.3390/ijerph16061060

32. Nicolais, L. and Pickering, S.J. (2012). Recycling Thermoset Composite Materials. In Wiley Encyclopedia of Composites, L. Nicolais (Ed.). https://doi.org/10.1002/9781118097298.weoc214
33. Job, S., Leeke, G., Mativenga, P. T., Oliveux, G., Pickering, S. J., & Shuaib, N. A. (2016). Composites recycling : Where are we now ?, 11. Retrieved from https://compositesuk.co.uk/system/files/documents/Recycling Report 2016_1.pdf
34. Nguyen, T.-C., Huynh, T.-C., & Kim, J.-T. (2015). Numerical evaluation for vibration-based damage detection in wind turbine tower structure. Wind and Structures, 21(6), 657–675. https://doi.org/10.12989/was.2015.21.6.657
35. Mishnaevsky, L., Branner, K., Petersen, H., Beauson, J., McGugan, M., & Sørensen, B. (2017b). Materials for Wind Turbine Blades: An Overview. Materials, 10(11), 1285. https://doi.org/10.3390/ma10111285
36. Zhang, K., Gu, Y., Zhang, J., Li, M., Wang, S., & Zhang, Z. (2015). Rapid curing vacuum-assisted resin infusion molding using silicone rubber sheet heater and the effect of cooling process on the properties of carbon fiber/epoxy composites. Journal of Composite Materials, 50(13), 1837–1850. https://doi.org/10.1177/0021998315597990
37. A. (2017). Unsustainable: 43 Million Tonnes Of Wind Turbine Blade Waste By 2050. Aletho News. https://alethonews.com/2017/06/22/unsustainable-43-million-tonnes-of-wind-turbine-blade-waste-by-2050
38. Lay, K. (2014). Wind turbine blades could be thrown into landfill, study warns. The Times. https://www.thetimes.co.uk/article/wind-turbine-blades-could-be-thrown-into-landfill-study-warns-276cm03tz03
39. Red, C. (2008, June 1). Wind turbine blades: Big and getting bigger. CompositesWorld. https://www.compositesworld.com/articles/wind-turbine-blades-big-and-getting-bigger
40. Albers, H, Greiner, S, Seifert, H, & Kuehne, U.(2009). Recycling of wind turbine rotor blades. Fact or fiction?; Recycling von Rotorblaettern aus Windenergieanlagen. Fakt oder Fiktion?. Germany.
41. Andersen, P. D., Bonou, A., Beauson, J., & Brøndsted, P. (2014). Recycling of wind turbines. In H. Hvidtfeldt Larsen, & L. Sønderberg Petersen (Eds.), DTU International Energy Report 2014: Wind energy — drivers and barriers for higher shares of wind in the global power generation mix (pp. 91-97). Technical University of Denmark.
42. Wang, S., Xing, X., Zhang, X., Wang, X., & Jing, X. (2018). Room-temperature fully recyclable carbon fibre reinforced phenolic composites through dynamic covalent boronic ester bonds. Journal of Materials Chemistry A, 6(23), 10868–10878. https://doi.org/10.1039/c8ta01801d
43. Weng, M.-C., Lin, C.-L., & Ho, C.-I. (2010). Mechanical properties of incineration bottom ash: The influence of composite species. Waste Management, 30(7), 1303–1309. https://doi.org/10.1016/j.wasman.2009.11.010
44. Griffith, K., & A. (2020). Hundreds of non-recyclable fiberglass wind turbine blades are pictured piling up in landfill. Mail Online. https://www.dailymail.co.uk/news/article-8294057/Hundreds-non-recyclable-fiberglass-wind-turbine-blades-pictured-piling-landfills.html

45. Asmatulu, E., Twomey, J., & Overcash, M. (2013). Recycling of fiber-reinforced composites and direct structural composite recycling concept. Journal of Composite Materials, 48(5), 593–608. https://doi.org/10.1177/0021998313476325
46. Vijay, N., Rajkumara, V., & Bhattacharjee, P. (2016). Assessment of Composite Waste Disposal in Aerospace Industries. Procedia Environmental Sciences, 35, 563–570. https://doi.org/10.1016/j.proenv.2016.07.041
47. Park, C. H., Jeon, H. S., Yu, H. S., Han, O. H., & Park, J. K. (2008). Application of electrostatic separation to the recycling of plastic wastes: Separation of PVC, PEL and ABS. Environmental Science and Technology, 42(1), 249-255. https://doi.org/10.1021/es070698h
48. Yoon, R. H. (2002). Recent development in plastics recycling in the U.S. Processing International Symposium on Establishment of Resource Recycling Society, Seoul, Korea.
49. Pascoe, R. D., & O'Connell, B. (2003). Development of a method for separation of PVC and PET using flame treatment and flotation. Minerals Engineering, 16(11), 1205–1212. https://doi.org/10.1016/s0892-6875(03)00171-7
50. Gonzalo Martínez-Barrera, Nelly González-Rivas, Enrique Vigueras-Santiago, Ángel Martínez-López, Jorge A. Tello-González and Carmina Menchaca-Campos. (2016). Waste and Recycled Materials and their Impact on the Mechanical Properties of Construction Composite Materials, Composites from Renewable and Sustainable Materials, Matheus Poletto, IntechOpen, https://doi.org/10.5772/65433
51. Feih, S., Boiocchi, E., Mathys, G., Mathys, Z., Gibson, A. G., & Mouritz, A. P. (2011). Mechanical properties of thermally-treated and recycled glass fibres. Composites Part B: Engineering, 42(3), 350–358. https://doi.org/10.1016/j.compositesb.2010.12.020
52. Goodship, V. (2010). Management, Recycling and Reuse of Waste Composites (Woodhead Publishing Series in Composites Science and Engineering) (1st ed.). Woodhead Publishing.
53. Hopewell, J., Dvorak, R., & Kosior, E. (2009). Plastics recycling: challenges and opportunities. Philosophical Transactions of the Royal Society B: Biological Sciences, 364(1526), 2115–2126. https://doi.org/10.1098/rstb.2008.0311
54. Pickering, Sj & Turner, Ta & Meng, Fanran & Morris, Cn & Heil, Jp & Wong, Kh & Melendi, S. (2015). Developments in the fluidised bed process for fibre recovery from thermoset composites.
55. Brydson, J. A. (1999). Plastics Materials (7th ed.). Butterworth-Heinemann.
56. Caballero, B. M., de Marco, I., Adrados, A., López-Urionabarrenechea, A., Solar, J., & Gastelu, N. (2016). Possibilities and limits of pyrolysis for recycling plastic rich waste streams rejected from phones recycling plants. Waste Management, 57, 226–234. https://doi.org/10.1016/j.wasman.2016.01.002
57. Miandad R, Rehan M, Barakat MA, Aburiazaiza AS, Khan H, Ismail IMI, Dhavamani J, Gardy J, Hassanpour A and Nizami A-S (2019) Catalytic Pyrolysis of Plastic Waste: Moving Toward Pyrolysis Based Biorefineries. Front. Energy Res. 7:27. https://doi.org/10.3389/fenrg.2019.00027
58. Yang, Y., Boom, R., Irion, B., van Heerden, D.-J., Kuiper, P., & de Wit, H. (2012). Recycling of composite materials. Chemical Engineering and Processing: Process Intensification, 51, 53–68. https://doi.org/10.1016/j.cep.2011.09.007

59. Cunliffe, A. M., Jones, N., & Williams, P. T. (2003). Pyrolysis of composite plastic waste. Environmental Technology, 24(5), 653–663. https://doi.org/10.1080/09593330309385599
60. Ignatyev, I. A., Thielemans, W., & Vander Beke, B. (2014). Recycling of Polymers: A Review. ChemSusChem, 7(6), 1579–1593. https://doi.org/10.1002/cssc.201300898
61. Kumar, S., & Krishnan, S. (2020). Recycling of carbon fiber with epoxy composites by chemical recycling for future perspective: a review. Chemical Papers, 74(11), 3785–3807. https://doi.org/10.1007/s11696-020-01198-y
62. Goto, M. (2009). Chemical recycling of plastics using sub- and supercritical fluids. The Journal of Supercritical Fluids, 47(3), 500–507. https://doi.org/10.1016/j.supflu.2008.10.011
63. Li, J., Xu, P.-L., Zhu, Y.-K., Ding, J.-P., Xue, L.-X., & Wang, Y.-Z. (2012). A promising strategy for chemical recycling of carbon fiber/thermoset composites: self-accelerating decomposition in a mild oxidative system. Green Chemistry, 14(12), 3260. https://doi.org/10.1039/c2gc36294e
64. Ma, Y., & Nutt, S. (2018). Chemical treatment for recycling of amine/epoxy composites at atmospheric pressure. Polymer Degradation and Stability, 153, 307–317. https://doi.org/10.1016/j.polymdegradstab.2018.05.011
65. Tofail, S. A. M., Koumoulos, E. P., Bandyopadhyay, A., Bose, S., O'Donoghue, L., & Charitidis, C. (2018). Additive manufacturing: scientific and technological challenges, market uptake and opportunities. Materials Today, 21(1), 22–37. https://doi.org/10.1016/j.mattod.2017.07.001
66. Liu, Z., Wang, Y., Wu, B., Cui, C., Guo, Y., & Yan, C. (2019). A critical review of fused deposition modeling 3D printing technology in manufacturing polylactic acid parts. The International Journal of Advanced Manufacturing Technology, 102(9–12), 2877–2889. https://doi.org/10.1007/s00170-019-03332-x
67. Quan, H., Zhang, T., Xu, H., Luo, S., Nie, J., & Zhu, X. (2020). Photo-curing 3D printing technique and its challenges. Bioactive Materials, 5(1), 110–115. https://doi.org/10.1016/j.bioactmat.2019.12.003
68. Prakash, K. S., Nancharaih, T., & Rao, V. V. S. (2018). Additive Manufacturing Techniques in Manufacturing -An Overview. Materials Today: Proceedings, 5(2), 3873–3882. https://doi.org/10.1016/j.matpr.2017.11.642
69. A. (2020, September 16). Stereolithography / SLA 3D Printing – Simply Explained. All3DP. https://all3dp.com/2/stereolithography-3d-printing-simply-explained/
70. Mwema, F. M., & Akinlabi, E. T. (2020). Basics of Fused Deposition Modelling (FDM). Fused Deposition Modeling, 1–15. https://doi.org/10.1007/978-3-030-48259-6_1
71. Tekinalp, H. L., Kunc, V., Velez-Garcia, G. M., Duty, C. E., Love, L. J., Naskar, A. K., Blue, C. A., & Ozcan, S. (2014). Highly oriented carbon fiber–polymer composites via additive manufacturing. Composites Science and Technology, 105, 144–150. https://doi.org/10.1016/j.compscitech.2014.10.009
72. Abeykoon, C., Sri-Amphorn, P., & Fernando, A. (2020). Optimization of fused deposition modeling parameters for improved PLA and ABS 3D printed structures. International Journal of Lightweight Materials and Manufacture, 3(3), 284–297. https://doi.org/10.1016/j.ijlmm.2020.03.003

73. Farahikia, M., Macwan, S., Delfanian, F., & Hu, Z. (2012). Evaluating the Mechanical Properties of Carbon Fiber Reinforced Polymer Matrix Composite Materials at Room and Elevated Temperatures. Volume 3: Design, Materials and Manufacturing, Parts A, B, and C, 1151–1158. https://doi.org/10.1115/imece2012-85671
74. Shofner, M. L., Lozano, K., Rodríguez-Macías, F. J., & Barrera, E. V. (2003). Nanofiber-reinforced polymers prepared by fused deposition modeling. Journal of Applied Polymer Science, 89(11), 3081–3090. https://doi.org/10.1002/app.12496
75. Mallick, P.K. (2007). Fiber-Reinforced Composites: Materials, Manufacturing, and Design, Third Edition (3rd ed.). CRC Press. https://doi.org/10.1201/9781420005981
76. Aruan Efendy, M. G., & Pickering, K. L. (2019). Comparison of strength and Young modulus of aligned discontinuous fibre PLA composites obtained experimentally and from theoretical prediction models. Composite Structures, 208, 566–573. https://doi.org/10.1016/j.compstruct.2018.10.057
77. Katchy, E.M. (2008). Introduction to Polymer Technology Second edition .EL „DEMAK Publishers. Enugu. Nigeria.
78. Mackenzie, J. K. (1950). The Elastic Constants of a Solid containing Spherical Holes. Proceedings of the Physical Society. Section B, 63(1), 2–11. https://doi.org/10.1088/0370-1301/63/1/302
79. Affdl, J. C. H., & Kardos, J. L. (1976). The Halpin-Tsai equations: A review. Polymer Engineering and Science, 16(5), 344–352. https://doi.org/10.1002/pen.760160512
80. Cox, H.L. (1952). The elasticity and strength of paper and other fibrous materials. British Journal of Applied Physics 3(3), pages 72-79.
81. Shuaib, N. A., & Mativenga, P. T. (2016). Energy demand in mechanical recycling of glass fibre reinforced thermoset plastic composites. Journal of Cleaner Production, 120, 198–206. https://doi.org/10.1016/j.jclepro.2016.01.070
82. Humboldt, Economy Sieve Shaker. (2016). [Illustration]. https://www.humboldtmfg.com/humboldt-motorized-economy-sieve-shaker.html
83. Nikon Eclipse E200 Microscope Cutaway Diagram. (2001, February 13). [Illustration]. https://micro.magnet.fsu.edu/primer/anatomy/nikone200cutaway.html
84. de Macedo, J. R. N., & dos Santos Rosa, D. (2015). Effect of Fiber and Starch Incorporation in Biodegradation of PLA-TPS-Cotton Composites. Key Engineering Materials, 668, 54–62. https://doi.org/10.4028/www.scientific.net/kem.668.54
85. Ramalingam, M., & Ramakrishna, S. (2017). Nanofiber Composites for Biomedical Applications (1st ed.). Woodhead Publishing.
86. A. Ávila-Orta, C., González-Morones, P., Agüero- Valdez, D., González-Sánchez, A., G. Martínez-Colunga, J., M. Mata-Padilla, J., & J. Cruz-Delgado, V. (2019). Ultrasound-Assisted Melt Extrusion of Polymer Nanocomposites. Nanocomposites - Recent Evolutions, 1. https://doi.org/10.5772/intechopen.80216
87. Chellamuthu, Sabarinathan & Muthu, S. & Ali, M. (2012). Experimental study on tensile behavior of multi wall carbon nanotube reinforced epoxy composites. Journal of Applied Sciences Research, 8, 3253-3259.
88. Rahimizadeh, A., Kalman, J., Fayazbakhsh, K., & Lessard, L. (2019). Recycling of fiberglass wind turbine blades into reinforced filaments for use in Additive Manufacturing.

Composites Part B: Engineering, 175, 107101. https://doi.org/10.1016/j.compositesb.2019.107101
89. Rahimizadeh, A., Kalman, J., Henri, R., Fayazbakhsh, K., & Lessard, L. (2019). Recycled Glass Fiber Composites from Wind Turbine Waste for 3D Printing Feedstock: Effects of Fiber Content and Interface on Mechanical Performance. Materials, 12(23), 3929. https://doi.org/10.3390/ma12233929
90. Rahimizadeh, A., Tahir, M., Fayazbakhsh, K., & Lessard, L. (2020). Tensile properties and interfacial shear strength of recycled fibers from wind turbine waste. Composites Part A: Applied Science and Manufacturing, 131, 105786. https://doi.org/10.1016/j.compositesa.2020.105786
91. Stoof, D., & Pickering, K. (2018). Sustainable composite fused deposition modelling filament using recycled pre-consumer polypropylene. Composites Part B: Engineering, 135, 110–118. https://doi.org/10.1016/j.compositesb.2017.10.005
92. Sherif, G., Chukov, D. I., Tcherdyntsev, V. V., Torokhov, V. G., & Zherebtsov, D. D. (2020). Effect of Glass Fibers Thermal Treatment on the Mechanical and Thermal Behavior of Polysulfone Based Composites. Polymers, 12(4), 902. https://doi.org/10.3390/polym12040902
93. Grause, G., Mochizuki, T., Kameda, T., & Yoshioka, T. (2012). Recovery of glass fibers from glass fiber reinforced plastics by pyrolysis. Journal of Material Cycles and Waste Management, 15(2), 122–128. https://doi.org/10.1007/s10163-012-0101-x
94. OTTO, W. I. L. L. I. A. M. H. (1961). Compaction Effects in Glass Fibers. Journal of the American Ceramic Society, 44(2), 68–72. https://doi.org/10.1111/j.1151-2916.1961.tb15352.x
95. Paramonov, Y., & Andersons, J. (2007). A family of weakest link models for fiber strength distribution. Composites Part A: Applied Science and Manufacturing, 38(4), 1227–1233. https://doi.org/10.1016/j.compositesa.2006.06.004
96. Ginder, R. S., & Ozcan, S. (2019). Recycling of Commercial E-glass Reinforced Thermoset Composites via Two Temperature Step Pyrolysis to Improve Recovered Fiber Tensile Strength and Failure Strain. Recycling, 4(2), 24. https://doi.org/10.3390/recycling4020024
97. Zhuang, R.-C., Burghardt, T., & Mäder, E. (2010). Study on interfacial adhesion strength of single glass fibre/polypropylene model composites by altering the nature of the surface of sized glass fibres. Composites Science and Technology, 70(10), 1523–1529. https://doi.org/10.1016/j.compscitech.2010.05.009
98. Ryu, S.-R., & Lee, D.-J. (2001). Effects of fiber aspect ratio, fiber content, and bonding agent on tensile and tear properties of short-fiber reinforced rubber. KSME International Journal, 15(1), 35–43. https://doi.org/10.1007/bf03184796
99. Etcheverry, M., & Barbosa, S. E. (2012). Glass Fiber Reinforced Polypropylene Mechanical Properties Enhancement by Adhesion Improvement. Materials, 5(12), 1084–1113. https://doi.org/10.3390/ma5061084
100. Frenzel, H., Bunzel, U., Häßler, R., & Pompe, G. (2000). Influence of different glass fiber sizings on selected mechanical properties of PET/glass composites. Journal of Adhesion Science and Technology, 14(5), 651–660. https://doi.org/10.1163/156856100742906

101. Krishnaprasad, R., Veena, N. R., Maria, H. J., Rajan, R., Skrifvars, M., & Joseph, K. (2009). Mechanical and Thermal Properties of Bamboo Microfibril Reinforced Polyhydroxybutyrate Biocomposites. Journal of Polymers and the Environment, 17(2), 109–114. https://doi.org/10.1007/s10924-009-0127-x
102. Faruk, O., Bledzki, A. K., Fink, H.-P., & Sain, M. (2012). Biocomposites reinforced with natural fibers: 2000–2010. Progress in Polymer Science, 37(11), 1552–1596. https://doi.org/10.1016/j.progpolymsci.2012.04.003
103. Kim, H. G. (2008). Effects of fiber aspect ratio evaluated by elastic analysis in discontinuous composites. Journal of Mechanical Science and Technology, 22(3), 411–419. https://doi.org/10.1007/s12206-007-1208-1
104. Osoka, Emmanuel & Onukwuli, Okechukwu. (2018). A Modified Halpin-Tsai Model for Estimating the Modulus of Natural Fiber Reinforced Composites, 1*, 7, pages 63-70.
105. Fu, S. (1996). Effects of fiber length and fiber orientation distributions on the tensile strength of short-fiber-reinforced polymers. Composites Science and Technology, 56(10), 1179–1190. https://doi.org/10.1016/s0266-3538(96)00072-3.